

ACTIVATION OF LARGE IONS IN FT-ICR MASS SPECTROMETRY

Julia Laskin* and Jean H. Futrell

Fundamental Science Directorate, Pacific Northwest National Laboratory,
P.O. Box 999 (K8-88), Richland, Washington 99352

Received 20 August 2003; received (revised) 21 November 2003; accepted 24 November 2003

Published online in Wiley InterScience (www.interscience.wiley.com) DOI 10.1002/mas.20012

The advent of soft ionization techniques, notably electrospray and laser desorption ionization methods, has enabled the extension of mass spectrometric methods to large molecules and molecular complexes. This both greatly extends the applications of mass spectrometry and makes the activation and dissociation of complex ions an integral part of these applications. This review emphasizes the most promising methods for activation and dissociation of complex ions and presents this discussion in the context of general knowledge of reaction kinetics and dynamics largely established for small ions. We then introduce the characteristic differences associated with the higher number of internal degrees of freedom and high density of states associated with molecular complexity. This is reflected primarily in the kinetics of unimolecular dissociation of complex ions, particularly their slow decay and the higher energy content required to induce decomposition—the kinetic shift (KS). The longer trapping time of Fourier transform ion cyclotron resonance mass spectrometry (FT-ICR MS) significantly reduces the KS, which presents several advantages over other methods for the investigation of dissociation of complex molecules. After discussing general principles of reaction dynamics related to collisional activation of ions, we describe conventional ways to achieve single- and multiple-collision activation in FT-ICR MS. Sustained off-resonance irradiation (SORI)—the simplest and most robust means of introducing the multiple collision activation process—is discussed in greatest detail. Details of implementation of this technique, required control of experimental parameters, limitations, and examples of very successful application of SORI-CID are described. The advantages of high mass resolving power and the ability to carry out several stages of mass selection and activation intrinsic to FT-ICR MS are demonstrated in several examples. Photodissociation of ions from small molecules can be effected using IR or UV/vis lasers and generally requires tuning lasers to specific wavelengths and/or utilizing high flux, multiphoton excitation to match energy levels in the ion. Photodissociation of complex ions is much easier to accomplish from the basic physics perspective. The quasi-continuum of vibrational states at room temperature makes it very easy to pump relatively large amounts of energy into complex ions and infrared multiphoton dissociation (IRMPD) is a powerful technique for characterizing large ions, particularly biologically relevant molecules. Since both SORI-CID and IRMPD are slow activation methods they have many common

characteristics. They are also distinctly different because SORI-CID is intrinsically selective (only ions that have a cyclotron frequency close to the frequency of the excitation field are excited), whereas IRMPD is not (all ions that reside on the optical path of the laser are excited). There are advantages and disadvantages to each technique and in many applications they complement each other. In contrast with these slow activation methods, the less widely appreciated activation method of surface induced dissociation (SID) appears to offer unique advantages because excitation in SID occurs on a sub-picosecond time scale, instantaneously relative to the observation time of any mass spectrometer. Internal energy deposition is quite efficient and readily adjusted by altering the kinetic energy of the impacting ion. The shattering transition—instantaneous decomposition of the ion on the surface—observed at high collision energies enables access to dissociation channels that are not accessible using SORI-CID or IRMPD. Finally, we discuss some approaches for tailoring the surface to achieve particular aims in SID. © 2004 Wiley Periodicals, Inc., *Mass Spec Rev* 24:135–167, 2005

Keywords: FT-ICR mass spectrometry; SORI-CID; multiple-collision activation; surface-induced dissociation; infrared multiphoton dissociation; large ions

I. INTRODUCTION

The development of soft ionization techniques such as electrospray (ESI) (Fenn et al., 1989) and matrix-assisted laser desorption ionization (MALDI) (Hillenkamp et al., 1991) resulted in an explosive growth of studies that utilize mass spectrometry for identification and structural characterization of large molecules. The most common strategy in these studies involves tandem mass spectrometry (MS/MS), which relies on structurally specific fragmentation of mass-selected ions in the gas phase. Typical MS/MS experiments involve mass selection of the ion of interest in the first MS stage and excitation of the ion followed by its dissociation and mass analysis of the resulting fragment ions in the second MS stage. In early studies of structures of small polyatomic ions, the ionization step often resulted in sufficient ion excitation for dissociation. However, both ESI and MALDI mainly produce molecular ions with very little, if any, fragmentation. It follows that the ion activation step is of crucial importance for MS/MS studies of large molecules.

It is well known that polyatomic ions require excess internal energy above their dissociation threshold to fragment on the time scale of a mass spectrometer. This excess internal energy is called the kinetic shift (KS) (Lifshitz, 1992; Lifshitz, 2002). Conventionally ions were excited by single collisions with neutrals or by absorption of one photon in the UV range. However, with

Contract grant sponsor: Office of Basic Energy of US Department of Energy; Contract grant number: 40457.

*Correspondence to: Julia Laskin, Fundamental Sciences Division, Pacific Northwest National Laboratory, P.O. Box 999 K8-88, Richland, WA 99352. E-mail: Julia.Laskin@pnl.gov

increasing size of the ion the KS increases dramatically, resulting in a dramatic decrease of dissociation rates. Consequently, efficient dissociation of large ions in a mass spectrometer requires deposition of large amounts of internal energy; this can be achieved only using multiple gas-phase collisions, multiphoton excitation, or collision with a suitably prepared surface. In multiple-collision activation or infrared multiphoton excitation the internal energy of the ion is increased in small increments and dissociation occurs when sufficient internal excitation is absorbed by the ion. These methods of ion activation—both slow heating methods—have been recently reviewed (McLuckey & Goeringer, 1997). The slow heating methods have been successfully used for identification both of relatively small and very large ions in FT-ICR MS.

An alternative approach introduced by Cooks and co-workers (Mabud, Dekrey, & Cooks, 1985; Cooks, Ast, & Mabud, 1990) relies on very fast, single-step excitation of the ion in collision with a surface, resulting in surface-induced dissociation (SID). A variety of processes occurring during interaction of both small and large ions with different surfaces have been extensively reviewed (Cooks, Ast, & Mabud, 1990; Dongre, Somogyi, & Wysocki, 1996; Grill et al., 2001; Jacobs, 2002). Physical and chemical properties of the surface play an important role in determining the outcome of the collision. In the range of ion kinetic energies utilized in SID studies, the major competing process with ion scattering off the surface is the neutralization of the precursor ion. More than 99% of projectile ions are neutralized in collisions with metal surfaces. However, organic surfaces (self-assembled monolayers (SAMs) of alkyl thiols on gold or thin organic films on metal substrates) are excellent targets for SID studies because of the reduced neutralization efficiency as compared to metal surfaces. Using these specialized surfaces, relatively high efficiency of internal excitation can easily be achieved (Cooks et al., 1994; Dongre, Somogyi, & Wysocki, 1996). Ion-surface collisions have been successfully used to induce fragmentation of peptides and proteins (Chorush et al., 1995; Dongre, Somogyi, & Wysocki, 1996).

The amount of internal energy required to observe ion dissociation (the dissociation threshold energy plus the KS) is strongly affected by the magnitude of the most probable rate constant sampled experimentally. Tandem-in-space mass spectrometers (Marzluff & Beauchamp, 1996) are characterized by short observation times (1–100 μsec) and large rate constants (10^4 – 10^6 sec^{-1}). Significantly lower rate constants (0.1 – 100 sec^{-1}) are sampled using trapping devices (tandem-in-time instruments). Because the KS decreases with observation time efficient dissociation of ions is easier to achieve in tandem-in-time instruments. In addition, tandem-in-time mass spectrometers enable multiple MS/MS (MS^n) experiments. Among the tandem-in-time instruments Fourier transform ion cyclotron resonance mass spectrometers (FT-ICR MS) offer very high mass resolving power,¹ which is extremely important for accurate

interpretation of MS/MS spectra of large molecules. Comprehensive reviews on principles and advances in FT-ICR mass spectrometry can be found elsewhere (see e.g., Amster, 1996; Dienes et al., 1996; Marshall, Hendrickson, & Jackson, 1998; Marshall, 2000; and references therein). It should be noted that “slow heating” methods are also commonly used in the quadrupole ion trap MS (McLuckey & Goeringer, 1997), which utilizes collision gas for confining ions in the center of the trap. This necessary presence of collision gas introduces additional cooling of excited ions by collisions with the bath gas as compared to activation in FT-ICR, where the only cooling mechanism for excited ions is by emission of infrared photons. However, this is the only fundamental difference between ion activation in FT-ICR and quadrupole MS.

This review will focus on the fundamental and practical aspects of the three aforementioned ion activation methods in FT-ICR MS: multiple-collision and multiphoton excitation, and ion activation by collisions with surfaces. We shall discuss the basic principles of all three techniques; highlight their advantages and disadvantages; discuss the optimal choice of the experimental conditions, and briefly outline the major factors that affect excitation efficiency. A comprehensive review on the efficiency of collisional activation in the FT-ICR MS can be found elsewhere (Laskin & Futrell, 2003a). We present a wide spectrum of possible applications of these activation techniques based on selected publications in this area. For additional information the readers are referred to more detailed reviews in the second part of this special issue.

II. MULTIPLE-COLLISION ACTIVATION (MCA-CID)

A. Fundamental Principles of Collisional Activation

Before discussing the variety of FT-ICR measurements and the relationships essential to interpreting this particular class of MS/MS measurements, we discuss briefly general characteristics of two body collisions relevant to energy exchange in collisional activation and deactivation of ions. Useful tutorials on the topic can be found elsewhere (McLuckey, 1992; Shukla & Futrell, 1993, 2000). We further relate the kinematic relationships to collisional activation (and deactivation) of ions that have been accelerated within the solenoid field of an ICR apparatus. Later in the text, we consider application of this class of experiments to ions colliding with a gold surface coated with a self-assembled monolayer for SID of impacting ions.

1. Reaction Kinematics

The simplest collision process, one that should be understood in at least broad aspects, is the elastic collision of structureless particles. The only outcome of such a collision is that the particles are deflected from their initial trajectories. This is nevertheless a complex problem to think about, involving $2 \times 3 = 6$ spatial coordinates as a function of time. Fortunately there are dramatically simplifying factors that enable a full description of particle motion before and after the collision in straightforward terms. Since the interparticle force—whatever the interaction potential

¹In this review, we use the term “mass resolution” to represent the amount of separation of two ions of similar mass obtained experimentally and the term “mass resolving power” to represent an instrument’s ability to separate two ions of similar mass, i.e., the ultimate mass resolution that can be obtained using a particular instrument. Both terms refer to $m/\Delta m$ at 50% height.

may be—for structureless particles is a central force and dependant only on separation R , the motion of the system is readily described as a combination of motion of the particles as a function of their relative separation with motion of the center of mass (CM) of the system. The motion of the CM has absolutely no effect on energy exchange or reaction and can be ignored for purposes of this discussion. It is relative motion of the particles within the moving CM reference frame that determines the outcome of the collision. The second important simplification, known since the time of Newton and Kepler, is that the collision of two particles characterized by a central force lies in a plane and all the properties of the collision can be defined by considering their relative motion in a plane. Both of these characteristics will be useful for understanding the description which follows.

In its simplest terms, the motion of the two particles in the CM frame may be described by conservation of linear momentum

$$m_1 u_1 + m_2 u_2 = 0, \quad (1)$$

where m_i and u_i are the masses and velocities of the two particles in the CM frame. The relative velocity is the difference between the two velocities

$$v = u_1 - u_2. \quad (2)$$

The relative kinetic energy in the CM frame (T_{CM}) is

$$T_{CM} = \frac{1}{2} m_1 u_1^2 + \frac{1}{2} m_2 u_2^2. \quad (3)$$

By substitution of Equations 1 and 2 into Equation 3 and using the definition for reduced mass for two interacting particles (μ)

$$\mu = \frac{m_1 m_2}{m_1 + m_2}, \quad (4)$$

one reaches the very important conclusion that

$$T_{CM} = \frac{1}{2} \mu v^2. \quad (5)$$

Energy is conserved and the total energy of the system (E_T) can be expressed as

$$E_T = T_{CM} + V(R) = \text{constant}, \quad (6)$$

where $V(R)$ is the potential energy acting between the particles. Since $V(R)$ is vanishingly small at large R , it is evident that the constant in Equation 6 is equal to T_{CM} defined in Equation 5 irrespective of the form of $V(R)$. This simple concept has relatively profound implications for collisional activation of ions. For example, the maximum possible energy transfer in a collision is the CM collision energy given by Equation 5. It follows that for collision of high mass ions with rare gases the maximum energy that can be deposited in a single collision decreases monotonically with increasing ion mass. Very rapidly the maximum possible energy transfer becomes too small to activate complex ions sufficiently to cause them to dissociate in the observation time of most mass spectrometers. From Equations 4 and 5 it is clear that the maximum energy transfer is larger for heavier collision gases.

Since $V(R)$ expresses the forces between the particles as they approach the turning point in their CM trajectories Equation 6 is a guide for understanding what actually happens in the collision process. Specifically this statement of the conservation of energy relationship implies that the form of the potential $V(R)$ governs changes in kinetic energy during the close encounter collision. For inelastic collisions the form of $V(R)$ influences both kinetic energy (through Eq. 6) and final trajectories of the particles. Angular momentum is conserved and there are analogous simplified relationships in CM coordinates for keeping track of angular momentum during a collision that will not be discussed here. Depending on impact parameter—separation of the line of centers at large separations—a centrifugal potential must be added that significantly influences the scattering of particles. These details are not essential to the discussion, which follows but are essential to describing and interpreting elastic, inelastic, and reactive collisions. For a more detailed discussion of these relationships, transformations of coordinates, centrifugal forces, cross sections, deflection functions and the like, the reader is directed to Levine & Bernstein (1987), Shirts (1986), and Futrell (1986).

Since the most detailed information on dynamics of energy exchange in gas phase collisions is obtained from crossed molecular beam studies, we summarize here the principles for interpreting crossed beam experiments conducted to explore energy transfer and mechanisms for collisional activation. The nature of those experiments is illustrated in cartoon form for the special case of collisions occurring at right angles in Figure 1. As noted earlier, no information is lost by carrying out the analysis in the collision plane. Further, the choice of right angle collisions is commonly made because it simplifies analysis

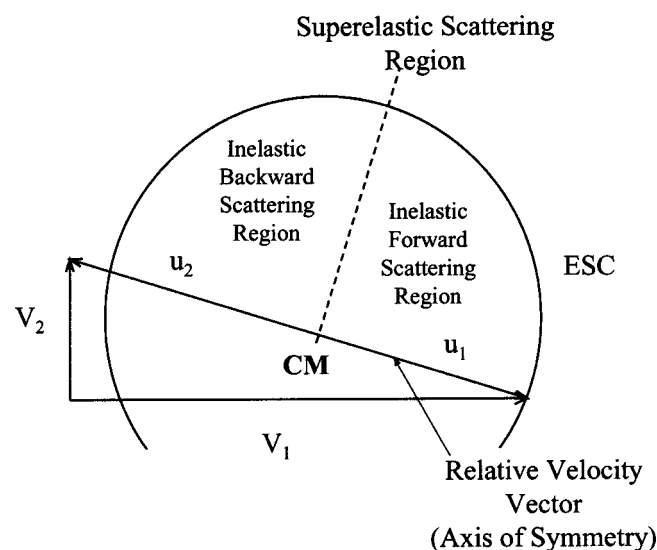


FIGURE 1. Newton diagram describing scattering dynamics in the center-of-mass (CM) reference frame. V_1 and V_2 represent velocity vectors of the ion and the neutral, respectively, in the laboratory frame. The corresponding CM velocities are denoted u_1 and u_2 . The diagram shows the elastic scattering circle (ESC) and the corresponding backward, forward and superelastic scattering regions.

by eliminating trigonometric cross terms in velocity transformations. It is convenient to consider Figure 1, a “post-collision” representation of a collision occurring at the origin with initial laboratory velocity vectors of the ion given by V_1 and the neutral by V_2 . The corresponding CM vectors of the ion u_1 and neutral u_2 are shown for the elastic scattering case in which the direction of the ion beam defines zero scattering angle. Note that the tip of the velocity vector of the ion in the laboratory frame coincides with the tip of the ion velocity vector in the CM frame, as it must. An important parameter in the figure is the elastic scattering circle (ESC) for the ion, ESC, which is the reference frame for classifying scattering processes. Ion velocity vectors located within the ESC are found for inelastic scattering, the normal case for collision-induced dissociation (CID) processes. Velocity vectors located outside the ESC correspond to superelastic scattering, resulting from the conversion of internal energy into translational energy. Forward scattering and backward scattering, which may involve identical energy conversion, are defined with respect to the initial CM velocity vector of the ion. What is usually found is a distribution of velocity vectors defining the range of energy exchanges and angular scattering mechanisms that take place. In favorable cases they may be interpreted in terms of specific mechanisms; three examples are shown below.

Since a wide range of laboratory energies and angles are accessible in scattering processes analysis in the CM framework is essential to defining whether a collision is elastic, inelastic, or superelastic. This is particularly important for the case where the particles leaving the CM have the same identity as the incoming particles, as in collisional activation and deactivation of ions, the main subject of this review. We have assumed atomic particles as the neutral collider in Figure 1 and have used this figure as a framework for collision induced dissociation processes. If the neutral has internal degrees of freedom, these are activated in the collision and a simple discussion of collisional activation is precluded. For this reason, we have restricted beam studies in our laboratory to rare gas collisions. Finally, we note that there is rotational symmetry about the CM relative velocity vector (u_1) in Figure 1. The CM relative velocity vector is, therefore, a symmetry axis for the scattering pattern in the scattering plane defined by vectors V_1 and V_2 . It is, therefore, sufficient to collect scattering data in either half of the scattering plane to determine the full scattering properties of the collision.

2. Application to Collisional Activation

From the basic physics of the CID process, we appreciate that it cannot be described as a two-body collision when three (or more) particles are formed as fragments. However, if we make the explicit assumption that there is a time delay between the collision step and the dissociation of the ion we can apply the kinematics considerations we have discussed. There are a number of reasons to believe this is a plausible assumption for gas phase collisions. The independence of activation and dissociation requires only that the recoiling ion and neutral escape the force field of the collision prior to dissociation. A plausibility argument can be advanced by considering that the relative velocities in CID activation of polyatomic ions below 100 Da is in the range of km/sec and interaction lengths are of the order of 10^{-9} m, leading to

an interaction time of tenths of picoseconds. The minimum time for ion dissociation to occur is many orders of magnitude longer if it follows RRKM kinetics (Shukla & Futrell, 1993, 2000); consequently the appropriate dynamics description is a two-body collisional activation step followed by unimolecular dissociation of the excited ion. For complex ions of principal interest in this review, the KS (discussed later) necessarily introduces a significant time delay into the dissociation process, further strengthening this assumption.

Alternative mechanisms have been considered and may indeed be important mechanisms for more complex ions than have been investigated thus far by beam methods. Before discussing this possibility further it is instructive to examine some examples of beam studies of CID. Figure 2 is the archetypical crossed beam study of a polyatomic ion CID reaction by Herman, Futrell, & Friedrich (1984). The reaction is the formation of methyl cations following collisional activation of the methane molecular cation. This was chosen for the first “test case” mechanistic study of CID because the large difference in mass of the methyl cation and H-atom enables use of measured CH_3^+ vectors as a surrogate for activated CH_4^+ . The conventions of Figure 1 are used along with an important question posed as to the operative mechanism in this early study—namely, whether the collisional activation involves activation of the entire methane molecular ion or a stripping reaction in which an H-atom is removed from the ion in the collision process. This is interrogated by plotting two distinct CM frames, one involving the collision of an H-atom with He and one involving collision of the entire ion. The two CMs are shown in Figure 2 along with experimental data defining the most probable velocities of methyl cations generated in the reaction. There is a range of forward scattering where the experimental data fall within both ESCs but a large number of points fall outside the CH_3^+ circle corresponding to the He/H CM ESC and within the He/ CH_4^+ ESC. There is no discontinuity in the experimental angular distribution indicating a change of mechanism. Moreover, the endothermicity of the reaction is consistent with an RRKM type mechanism in

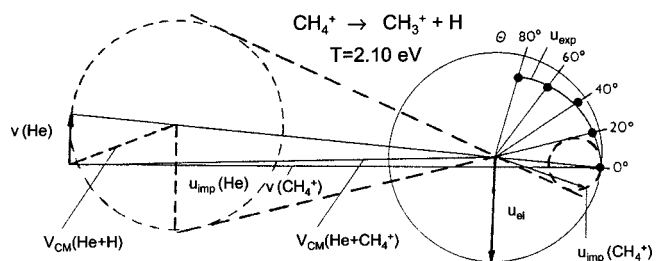


FIGURE 2. Newton diagram showing the most probable CM velocities of collisionally activated CH_4^+ on collision with He at 2.10 eV collision energy. The solid circle shows the locus of the CH_4^+ CM velocities (u_{el}) corresponding to the elastic scattering of CH_4^+ by He whereas the small broken circle shows the locus of CH_4^+ CM velocities expected from the spectator stripping mechanism where only the H atom takes part in the collision process. The large dashed circle locates the region where He and H are scattered. Reproduced from Herman, Futrell, & Friedrich (1984), with permission from Elsevier Science, copyright 1984.

which the translational energy converted into internal energy in the ion is fully available for dissociation.

We conclude from this pioneering study that CID reactions of polyatomic ions typically involve momentum conserving collisions of the entire ion with the neutral and energy shifts are to be interpreted as indicated in Figure 1—namely, endothermic reactions falling within the ESC constructed according to the rules indicated above. This is exactly what he have found in most cases investigated in our laboratory using the crossed beam method. In several cases, quantitative conclusions were possible about electronic excitation present in ions generated by electron impact or specific pathways for electronic excitation of ground state ions. Scattering angles observed in these studies support the interpretation that CID generally proceeds by impulsive mechanisms involving close encounters of the partners with recoil from the repulsive part of the potential describing their collision. This does not mean that all polyatomic ions proceed by such mechanisms, just that we find it to be generally true in cases examined thus far. An exception is triatomic ions for which we find an impulsive knock-out mechanism is a common dynamics mechanism for energy transfer (Shukla & Futrell, 2000).

Although the two-step model for CID has much to commend it an alternative kinematic mechanism is well established for both neutral and ion-molecule reaction dynamics, generally for small molecules. This model is prompt—instantaneous in the model—dissociation such that only a portion of the ion (an atom of small group of atoms) is involved in the momentum conserving collision. This spectator stripping or knockout model was proposed for CID of triatomics (Cheng et al., 1970) and more recently was suggested as an explanation for the observed very large kinetic energy shifts in activating high mass ions (Uggerud & Derrick, 1991) and for clusters (Woodward & Stace, 1991). Implicit in this model, which assumes components of the ion or neutral continue along their original trajectories unperturbed by the collision process, is the concept that the collision excites an initially bonding interaction to either a weakly bonded or weakly repulsive state which decouples the fragment ion without affecting the remainder of the ion. If this does not take place significant scattering of the “spectator” would necessarily occur from coupling of atomic motions in the dissociation step.

Experimental proof for a more elaborate version of the knockout model in which significant scattering occurs was obtained a few years ago in our laboratory (Tosh, Shukla, & Futrell, 1995). This is presented in the Figure 3 reactive scattering diagram for formation of S^+ in the collision of CS_2^+ with Ar constructed according to the principles illustrated in Figure 1. Shown in the figure are the ESC for CS_2^+ colliding with Ar and three scans at the indicated laboratory angles for S^+ scattering. We note parenthetically that CS_2^+ elastic scattering (not shown) follows precisely the ESC in Figure 2. Two CMs are shown in Figure 2, the conventional one assuming the reactant ion and Ar are the colliding partners and one assuming that S^+ collides with Ar. Since the dashed line circle through the perpendicular lines representing the most probable velocities of S^+ has the S^+ /Ar CM as its center, it is clear that the momentum conserving collision involves collision of S^+ with Ar and this CID process follows the basic assertion of the knockout model. A more detailed analysis (Tosh, Shukla, & Futrell, 1995) involving somewhat complex algebra and a large number of angular scans supports the con-

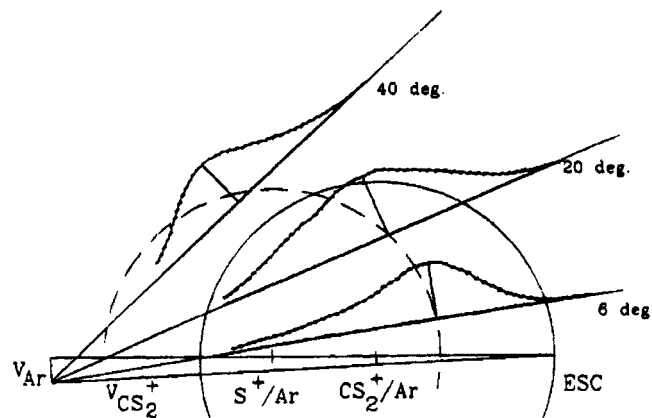


FIGURE 3. Angular scans of CS_2^+ intensity at selected angles of 7, 20, and 32°. Laboratory scattering angles referenced to Newton diagram for CS_2^+ scattering by Ar. Perpendicular lines dropped from maxima are referenced to the EX. Distributions of roughly equal height are obtained by multiplying the scans at 20 and 32° by factors of 5 and 500, respectively. Reproduced from Tosh, Shukla, & Futrell (1995), with permission from American Chemical Society, copyright 1995.

clusion that the $X^2\Pi_g$ state of CS_2^+ is excited in the momentum-conserving collision to the $B^2\Sigma_u^+$ state which then undergoes curve-crossing to the repulsive $^4\Sigma_-$ state. This decouples the strongly bound ground state (4.8 eV) to a flat to slightly repulsive state; this is essential to fulfill the second assumption of the knockout model that strongly attractive or repulsive forces are turned off in the collision.

An important point is that for this kinematically more complex case is that energy exchange can be fully deduced provided the initial velocity vectors of the colliding particles are known and the recoil velocity of any one of the product particles can be measured. This validates the power of the crossed beam method for determining details of energy exchange and mechanisms in collision induced dissociation. A second general point is that we have not found examples of polyatomic ions that follow the stripping or knockout model among the several cases we have examined in detail. Given that all crossed beam studies to date have dealt with ions of less than 100 Da this generalization is very unlikely to hold for much larger complex ions. Once ions become sufficiently large that interaction of the entire molecule becomes improbable it is plausible that interaction with only a small part of the molecular ion becomes the norm. Whether this is followed by energy randomization and unimolecular decay or a knockout mechanism is followed will be governed by the rate of energy exchange into internal modes. Smaller ESCs and reduced ion losses are likely consequences of these changes in dynamics.

3. Extension to Collision With Thermal Energy Neutrals

In each of the diagrams constructed and discussed above we have taken the velocities of the ion and neutral as delta functions. Actual experiments have to take into account the dispersion in velocities and angles of the reactant beams. Taken together these uncertainties define the minimum region in Cartesian velocity

space where fragments may be found. In non-beam experiments for which the neutral collision partner typically has a thermal distribution of velocities significant smearing of product velocities may result. For CID this is minimized by higher ion mass and velocities and by lower mass and lower temperatures for the collision neutral. For FT-ICR measurements of interest in this review, the problem is particularly severe and particularly difficult to describe or model in detail. This will be illustrated by first considering the collision in which a neutral moving with average thermal velocity at 300 K collides at right angles [as in the above illustrations] with an ion at an energy typical of ICR experiments and in the absence of a magnetic field.

Figure 4 is such an idealized Newton diagram for the collision of an ion of mass 500 Da and 10 eV kinetic energy with thermal Ar atoms at a right angle. Since this is a velocity diagram the neutral has a velocity about twice as large as the ion velocity. However, the CM of the collision is much closer to the ion velocity vector tip. The construction of the ESC in the usual way leads to the interesting conclusion that ions may be scattered by as much as $\pm 43^\circ$ in such a collision. This diagram is not intended to represent the dynamics of collision with thermal energy particles in any realistic manner. Thermal velocities are a Boltzmann distribution and range from zero to much larger values than the average velocity chosen for Figure 4. Additionally the velocity vectors of the neutral have to be averaged over all collision orientations and have zero as their average. The point of the figure is that a range of large angle scattering results from typical collisions with neutrals moving at thermal velocities in drift tubes and collision chambers. A final caveat is that Figure 4 applies to

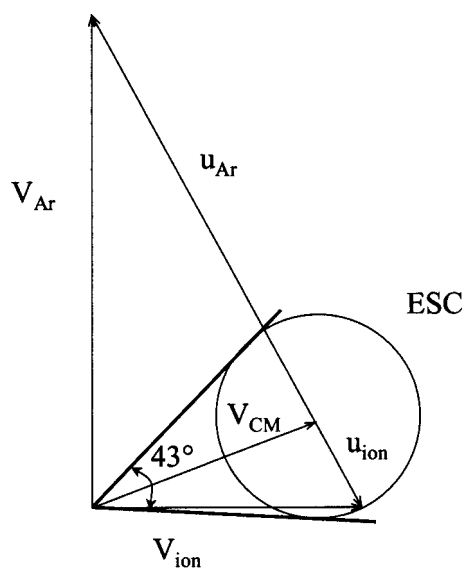


FIGURE 4. Newton diagram for the collision of an ion of mass 500 Da and 10 eV kinetic energy with thermal Ar atoms at a right angle. V_{Ar} , V_{ion} , and V_{CM} denote the velocity of neutral, ion and the CM, respectively, in the laboratory frame; u_{Ar} and u_{ion} denote the velocities of the neutral and the ion, respectively, in the CM reference frame. The ESC illustrates that under these conditions the maximum scattering angle is 43° .

elastic collisions and not to inelastic collisions that convert kinetic energy into internal energy. Both trajectory modeling (Meroueh & Hase, 1999) and experimental studies (Shukla & Futrell, 2000; Muntean & Armentrout, 2001; Laskin & Futrell, 2002) indicate that a broad range of energy exchange occurs in ion-neutral collisions and large angle scattering would certainly be observed if trapping fields were not present. The true picture for an FT-ICR CID experiment is far more complex, of course, than suggested by this simple diagram. Velocity vectors of the neutral would have to be averaged over all angles and over the velocity distribution at the temperature of the experiment. Most importantly, the magnetic field would very strongly constrain the vectors of the incoming and outgoing ion. However, the scattering properties suggested by Figure 4 are a mechanism for mixing cyclotron and magnetron motion of the ion resulting in the observed ion loss in FT-ICR CID experiments.

B. On-Resonance CID

Before the development of ion activation techniques described below collisional activation in FT-ICR was effected by applying a short rf pulse at the cyclotron frequency of the ion. The duration and the amplitude of this pulse determine the final kinetic energy of the ion. Ions are activated by collisions with neutral atoms or molecules inside the ICR cell. A comprehensive literature survey on the on-resonance CID can be found elsewhere (Dienes et al., 1996). It has been used to study fragmentation of relatively small ions under single-collision conditions. If multiple collisions occur, the kinetic energy of ions is effectively damped and the efficiency of subsequent collisions is small, limiting application of this method for dissociation of large ions. In addition, on-resonance excitation results in significant distortion of the ion cloud, thereby lowering the mass resolving power of the mass spectrometer. It has been shown that time domain data (transients) obtained using conventional CID last less than 1s (Senko, Speir, & McLafferty, 1994).

C. MCA-CID Techniques

The limitations of the on-resonance CID can be surmounted using different techniques for multiple-collision activation described in this section.

1. MECA

In multiple excitation collisional activation (MECA) (Lee et al., 1993) precursor ions that do not dissociate after the first excitation step are re-excited several times until dissociation occurs (Fig. 5). In each step, ions are resonantly excited to a relatively small radius and return to the center of the ICR cell by collisional relaxation. Fragmentation efficiency is significantly improved using this method. Furthermore, lower kinetic energies, which leave fragment ions closer to the center of the cell, are used in MECA compared to conventional CID. The average internal energy deposited into the ion in each step is determined by the average kinetic energy of the ion. Fragmentation efficiency can be improved using fewer excitations with higher voltages and

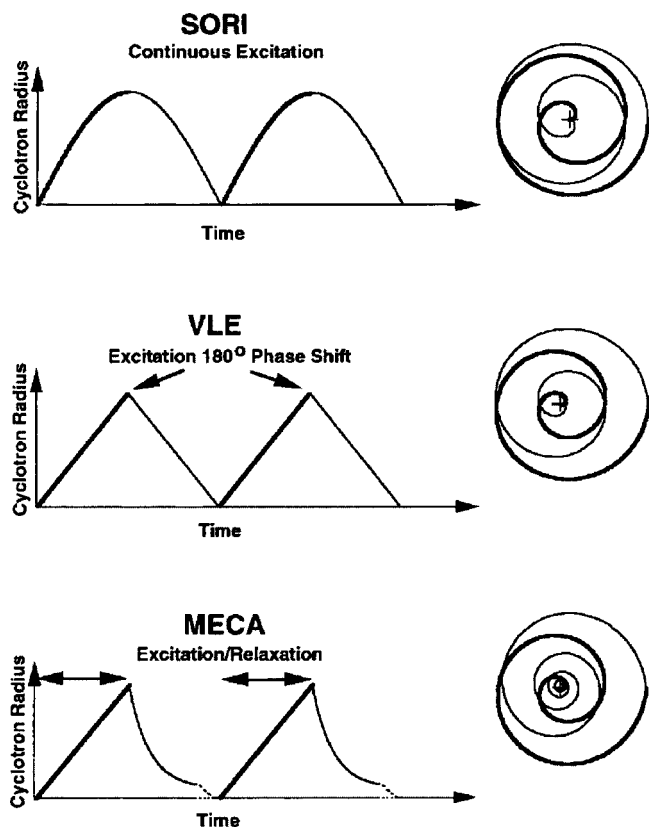


FIGURE 5. Time evolution of ion cyclotron radius (**left**) and ion xy-trajectory (**right**) for each of three ICR techniques for ion multiple activation based on repeated single-frequency dipolar excitation for collision induced dissociation (CID). In multiple excitation for collisional activation (MECA), ions are resonantly excited and then allowed to relax by collisions. In sustained off-resonance irradiation (SORI), ions are alternately excited and de-excited because of the difference between the excitation frequency and the ion cyclotron frequency. In very low energy (VLE) CID, ions are alternately excited and de-excited by resonant excitation whose phase alternates between 0 and 180°. Reproduced from Guan & Marshall (1996), with permission from Elsevier Science, copyright 1996.

longer delays between repetitions (Senko, Speir, & McLafferty, 1994). However, similarly to on-resonance CID, increasing the maximum kinetic energy of the ions will eventually result in significant distortion of the ion cloud.

2. VLE-CID

Similar ideas are utilized in very low energy collisional activation (VLE-CA) (Boering, Rolfe, & Brauman, 1992). In this method, sequential acceleration/deceleration is achieved using a 180° phase shift of the excitation waveform applied at the cyclotron frequency of the ion (Fig. 5). In contrast with MECA in VLE-CID ion motion is controlled by the rf field through the entire acceleration/deceleration step. The drawback of the VLE-CID is

that the abrupt phase inversion results in spikes in the frequency domain that cause further activation and possible ejection of fragment ions. A much “cleaner” waveform in the frequency domain is obtained by modulating the amplitude of the resonant frequency with a sine wave (Senko, Speir, & McLafferty, 1994). This leaves just two spikes in the frequency domain at the sum and the difference frequency of the activation and modulation waveforms. Resonant amplitude modulated RAM-CID (Senko, Speir, & McLafferty, 1994) produced very similar mass spectra to sustained off-resonance irradiation SORI-CID described in the next section.

3. SORI-CID

SORI (Gauthier, Trautman, & Jacobson, 1991) utilizes off-resonance excitation of the ion being investigated. An rf pulse is applied slightly above or below the resonant frequency of the precursor ion, causing the ion’s kinetic energy to oscillate with time (Fig. 5). Since ion kinetic energy oscillates with time and collisions occur randomly, the collision frequency at the maximum number density of the gas pulse should be high enough both to sample the full CM energy range and effectively average over all kinetic energies. On the other hand, the collision frequency should be low enough to avoid damping of the ion kinetic energy by collisions. To ensure multiple collisions the excitation pulse is, therefore, applied for a time much longer than the time between collisions. With multiple collisions of the translationally excited ion with the target gas its internal energy slowly increases and fragmentation occurs when sufficient energy is transferred from translational to internal energy. Similarly to other methods (MECA and VLE-CID) SORI-CID leaves fragment ions close to the center of the cell.

All three methods described above demonstrated highly efficient fragmentation of the +11 charge state of bovine ubiquitin (Senko, Speir, & McLafferty, 1994). However, MECA resulted in somewhat lower fragmentation efficiency and slightly different fragmentation pattern as compared to RAM- and SORI-CID (see Fig. 6). All three methods have similar drawbacks that are associated with introduction of the collision gas, unintentional excitation and ejection of fragment ions and distortions of isotope distributions of ions (which will be discussed later in this review). However, SORI-CID is by far the most robust and easy to implement activation technique and has found the most widespread application in the FT-ICR MS.

4. MCA-CID in an External Reservoir

Although this review is limited to activation techniques inside the ICR cell, it should be noted that efficient fragmentation of large ions can be also achieved in the external ion trap (Sannes-Lowery et al., 1998; Sannes-Lowery & Hofstadler, 2000; Wang et al., 2000). This approach eliminates the need to introduce collision gas into the ICR cell, which substantially increases the experimental duty cycle and enables faster data acquisition. Furthermore, many FT-ICR mass spectrometers are equipped with an external accumulation stage to enhance the ion current delivered into the ICR cell. It can, therefore, be conveniently used

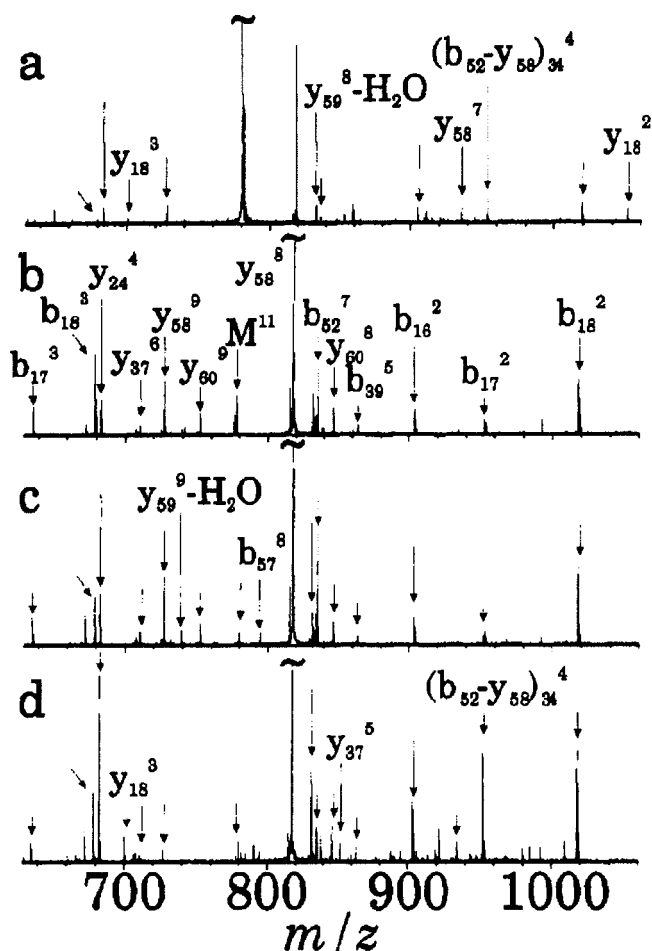


FIGURE 6. CAD spectra of $(M+11H)11+$ of bovine ubiquitin using (a) standard resonant excitation, (b) SORI, (c) RAM activation, and (d) MECA. All spectra are displayed at a relative abundance of 30% of the base peak. Reproduced from Senko, Speir, & McLafferty (1994), with permission from American Chemical Society, copyright 1994.

for fragmentation of the ions followed by mass analysis in the ICR cell.

D. Important Parameters for SORI-CID

1. Ion Kinetic Energy

The kinetic energy of the ions in the laboratory frame (E_{lab}) is given by (Sievers, Grutzmacher, & Caravatti, 1996):

$$E_{lab} = \frac{\beta^2 q^2 V_{p-p}^2}{16md^2 \Delta\omega^2} [1 - \cos(\omega - \omega_c)t], \quad (7)$$

where m and q are the mass and the charge of the ion, respectively; ω_c is the cyclotron frequency of the ion, ω is the frequency of the excitation field, $\Delta\omega = \omega - \omega_c$, V_{p-p} is the peak-

to-peak excitation voltage, d is the diameter of the cell, and β is the geometry factor (Grosshans & Marshall, 1990). The maximum kinetic energy (peak-to-peak) achieved by off-resonance CID is given by:

$$E_{lab}^{max} = \frac{\beta^2 q^2 V_{p-p}^2}{8md^2 \Delta\omega^2}. \quad (8)$$

Equations 7 and 8 differ by a factor of 1/2 from the equations given by Grosshans & Marshall (1990). This factor results from the fact that a dipolar excitation field can be described as the sum of two circularly polarized fields rotating in opposite senses and power absorption occurs only from the field component rotating in the same sense with the ion. The counter-rotating field has no net effect on ion motion.

From Equation 8, it is clear that the two major parameters that determine the maximum kinetic energy of the ions are the peak-to-peak voltage (V_{p-p}) and the offset (beat) frequency $\Delta\omega$. It should be noted that V_{p-p} in Equations 1 and 2 is often confused with the peak-to-peak voltage of the excitation waveform on the output of the power amplifier (V_{p-p}^{amp}). V_{p-p} in Equations 7 and 8 refers to the voltage actually applied across the plates of the ICR cell. Because each plate receives the original waveform shifted by 180° with respect to another plate V_{p-p} is twice as high as V_{p-p}^{amp} .

2. Number of Collisions Experienced by the Ion

For a monoenergetic ion beam colliding with neutral gas the probability that ion undergoes m collisions, Q_m , is given by the Poisson distribution (Kim, 1983):

$$Q_m = \frac{e^{-a} a^m}{m!}, \quad (9)$$

where $a = \nu t_{CID}$ is the average number of collisions during the CID delay t_{CID} for a collision frequency ν . The collision frequency is given by $\nu = \sigma n v$, where σ is the collision cross section, n is the number density of neutrals, and v is the velocity of the ion. For sufficiently large ions collision cross section is given by the physical size of the ion and is independent of ion velocity. The ion induced dipole interaction described by the Langevin potential (Levine & Bernstein, 1987) results in collision cross section that is inversely proportional to ion velocity. The Langevin cross-section depends on the polarizability of the neutral partner. For collision gases commonly used in CID experiments (e.g., Ar, N_2 , CO_2) the Langevin cross section (σ_L) becomes comparable to hard-spheres cross-section of large ions only at very low collision energies. For example, for collisions with Ar σ_L equals 216 \AA^2 at the CM collision energy of only 0.01 eV and rapidly decreases with increase in collision energy. This should be compared with typical collision cross sections for tryptic peptides that are in the range from 150 to 270 \AA^2 (Valentine et al., 1999).

The resultant distribution corresponding to $a = 10$ for an ideal case when ion kinetic energy does not change during the collision process is shown in Figure 7a. It is a symmetric bell-shaped function according to which ion undergoes on average ten collisions. However, in most situations ion kinetic energy is altered by collisions and by the excitation field. For example,

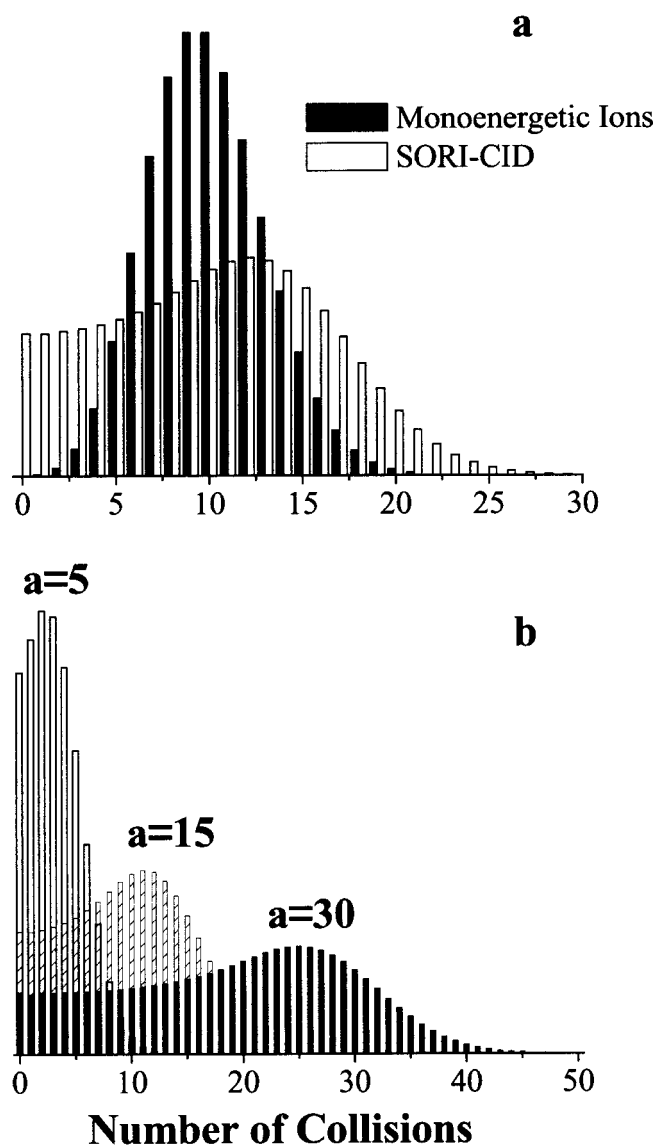


FIGURE 7. **a:** Distribution of the number of collisions for SORI-CID averaged over excitation time with ten collisions on average and the correspondent distribution for monoenergetic collisions for $a=10$; **b:** SORI-CID distributions of the number of collisions for $a=5, 15,$ and 30 .

during SORI ion velocity oscillates with time, resulting in the corresponding oscillation of the collision number (a) in Equation 9. In this case the distribution of the number of collisions can be obtained by averaging Q_m in Equation 9 over many oscillation periods (Laskin, Byrd, & Futrell, 2000). The resultant distribution calculated for 10 collisions on average is shown in Figure 7a. It is distinctly different from the distribution obtained for monoenergetic ions. Because the collision frequency for low-energy ions is much lower than the collision frequency for ions with high kinetic energy, the distribution for SORI excitation is

asymmetric with much higher weight for small numbers of collisions.

The number of collisions experienced by the ion can be varied experimentally by changing the pressure (therefore, the number density of neutral molecules) or by changing the velocity of the ion. Since collision frequency is proportional to ion velocity, increase in kinetic energy of the ion during SORI alters the number of collisions it experiences. It is, therefore, important to conduct experiments at the same average number of collisions in quantitative studies of the effect of ion's kinetic energy on the efficiency of SORI-CID.

The third parameter that affects the number of collisions is the collision cross section—an intrinsic property of the ion. For fixed pressure and maximum velocity of the ion during SORI increase in collision cross section of the ion results in the corresponding increase in the collision number (a). SORI distributions obtained for $a=5, 15,$ and 30 are shown in Figure 7b. The distributions mimic the effect of a threefold and sixfold increase in the collision cross section. Clearly, an increase in collision cross section has a profound effect on the distribution. It follows that accurate comparison of SORI-CID data obtained for different ions should be performed by conducting experiments with the same collision number.

E. Choice of Experimental Parameters for SORI-CID

1. Collision Gas and Pressure

For monoatomic gases the CID efficiency is expected to increase with increase in the mass of collision gas because of the corresponding increase in the CM collision energy (Eqs. 4 and 5), the maximum energy available for ion excitation. However, as explained previously part of the CM collision energy can be absorbed into vibrational excitation of the neutral for polyatomic targets. It follows that collision with molecular targets results in lower excitation of the ion. This effect is less pronounced if vibrational degrees of freedom of the neutral molecule constitute only a small fraction of the total vibrational degrees of freedom of the collision partners.

Collision gas can be admitted into the ICR cell using a leak valve or a pulsed valve. In the former case the static pressure in the cell is elevated, which allows for good control over the number density of the neutral molecules. The velocity of the ion, the collision frequency and the mass of the collision gas determine the practical range of static pressures for multiple-collision CID. For example, 1×10^{-7} Torr of argon is required to obtain 20 collisions per second with protonated pentaalanine for the CM collision energy of 5 eV (even higher pressure is required for activation of slower ions). However, as the static pressure in the cell increases, both sensitivity and resolution of the ICR degrade rapidly because of collisional damping of the ICR signal during the detection. In the above example ion activation should take approximately 20 sec to maintain a reasonably low pressure for signal acquisition. This presents a severe limitation for the static pressure approach, which has been utilized mainly for single-collision CID.

A more practical approach relies on pulsed introduction of the collision gas into the ICR cell. In this case, the fast rise in

pressure is followed by a long (2–5 sec) pump down delay. For pulsed gas introduction pressure calibration becomes more tedious. A standard routine that utilizes collisional damping of the ICR signal as a function of pressure is described elsewhere (Laskin, Byrd, & Futrell, 2000). Pressure profiles obtained on a 7 T Bruker BioApex instrument for two different opening times of the pulsed valve are shown in Figure 8. The profiles are very similar and show a fast increase in the pressure followed by a slow evacuation of the residual gas. The rise time of the profiles is longer than the opening time of the pulsed valve. For both opening times (5 and 50 msec) it takes approximately 80 msec for pressure to build up in the cell. Increase in the opening time of the valve from 5 to 50 msec results in a fivefold increase in the peak pressure.

The effect of the average number of collisions experienced by the ion on the energy transfer efficiency has been studied for bromobenzene radical cation (Laskin, Byrd, & Futrell, 2000). Figure 9 shows the dependence of the average energy deposited into the ion as a function of the peak pressure in the cell for different CM collision energies. At low CM energies, the average

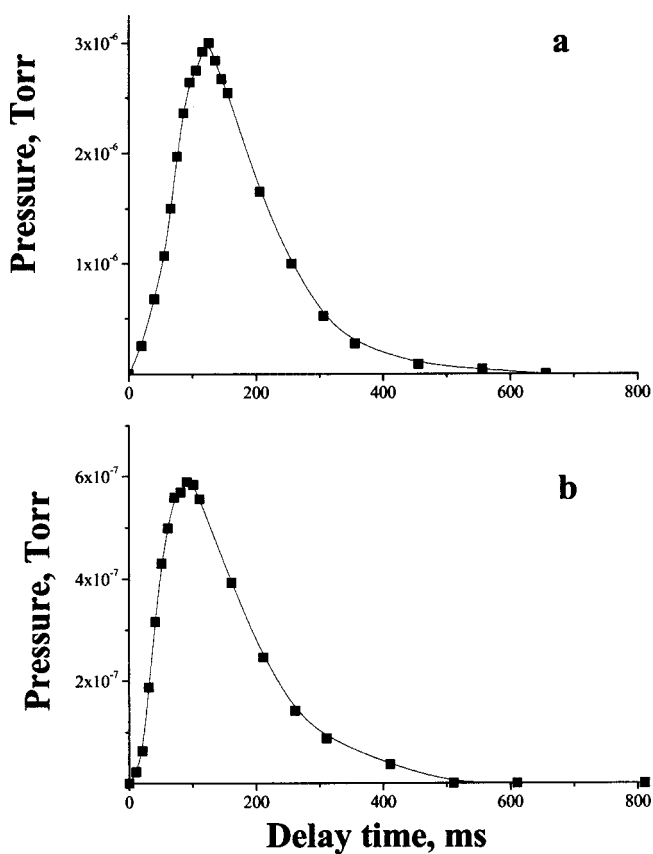


FIGURE 8. Pressure profiles obtained with backing pressure of 3.3 Torr and (a) 50 msec and (b) 5 msec valve open times. τ is the delay between pulse valve opening and the detection event. Reproduced from Laskin, Byrd, & Futrell (2000), with permission from Elsevier Science, copyright 2000.

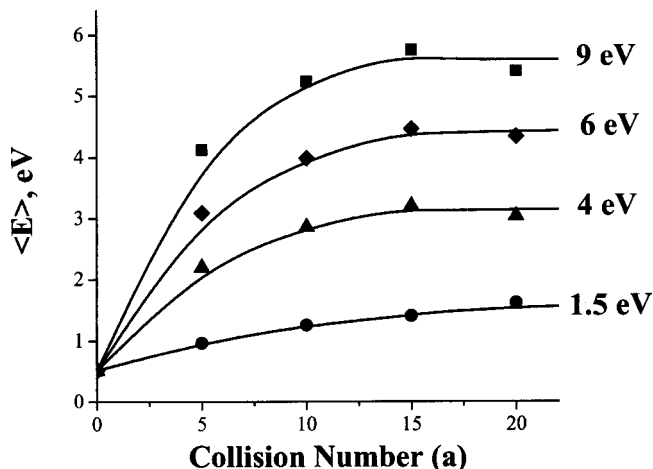


FIGURE 9. Average internal energy deposited into $C_6H_5Br^+$ in MCA-CID as a function of pressure for different collision energies. Reproduced from Laskin & Futrell (2003a), with permission from Wiley, copyright 2003.

energy of the ion population shows a very weak dependence on pressure. However, for higher CM energies the dependence on pressure becomes more pronounced. Energy transfer rises quickly at low pressures and levels off at high pressures. Further increase in pressure results only in excessive ion loss and does not increase energy transfer efficiency significantly. Similar results were obtained by Williams and co-workers for SORI-CID of protonated leucine enkephalin (Schnier, Jurchen, & Williams, 1999). In that study, it was suggested that leveling off occurs as a result of damping of the maximum kinetic energy of the ions when the collision frequency approaches the beat frequency. However, fragmentation efficiency for bromobenzene hardly changes when the number of collisions is increased from 20 to 100 while keeping the ratio between the beat (offset) frequency and the collision frequency constant (Laskin, Byrd, & Futrell, 2000). This experiment was done using one gas pulse and 100 msec irradiation time for 20-collision experiment and five gas pulses and 500 msec irradiation time for the 100-collision experiment.

2. Irradiation Time

Ion motion during the off-resonance excitation has been studied by several groups (Heck et al., 1991; Shin & Han, 1997; Schnier, Jurchen, & Williams, 1999). In the absence of collisions ions undergo repetitive acceleration/deceleration as a coherent packet. This results in oscillation of the peak height in the mass spectrum as a function of the irradiation time with characteristic beat frequency, $\Delta\omega$, corresponding to the difference between the reduced cyclotron frequency of the ion and the excitation frequency. Figure 10 shows the evolution of the ion signal as a function of irradiation time in the presence of the collision gas for the collision frequency of $\sim 230 \text{ sec}^{-1}$ (one collision per beat cycle). Oscillations in the ICR signal are very pronounced for the

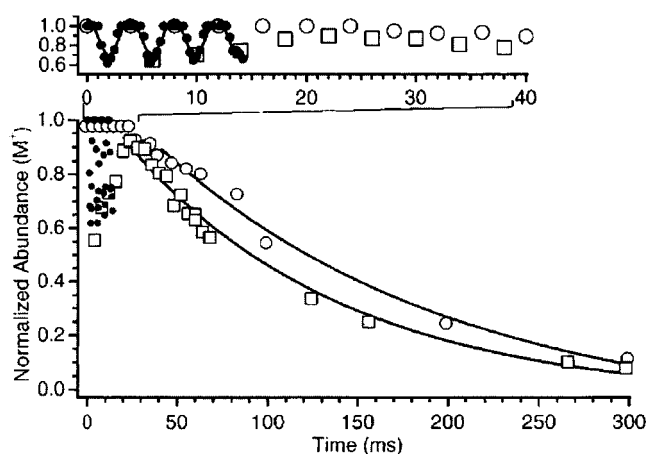


FIGURE 10. Normalized precursor ion abundance of protonated leucine enkephalin as a function of SORI excitation time. The open squares and open circles represent data points sampled at times in which the excitation waveform is stopped exactly when the irradiated ions have a maximum and minimum cyclotron radius, respectively. Reproduced from Schnier, Jurchen, & Williams (1999), with permission from American Chemical Society, copyright 1999.

short irradiation times and are damped as the time increases. This is a result of de-phasing of the initially coherent ion packet by collisions with background gas. Furthermore, the signal intensity is affected by the phase at which the excitation waveform is switched off. If the irradiation is stopped when ions have a maximum kinetic energy they undergo additional energetic collisions after SORI is switched off. This is reflected in a higher fragmentation efficiency obtained for the ions left with the maximum kinetic energy (open squares) versus the ions “parked” to the center of the cell (open circles) at the end of the irradiation period. From the above discussion, it follows that optimal irradiation time should be long enough to allow for dephasing of the coherent motion of the ion packet. In addition, it is important to control the phase at which the irradiation waveform is switched off.

It should be noted that the beat frequency of SORI can be accurately measured by following the oscillation in the ion signal as a function of irradiation time without adding collision gas (Shin & Han, 1997). The reduced cyclotron frequency can then be obtained from the known excitation frequency and measured beat frequency. Because the beat frequency is significantly lower than the cyclotron frequency of the ion and can be measured with very high precision this method enables extremely accurate mass determination.

In pulsed-gas experiments, the irradiation time is practically limited by the pressure profile. In our SORI-CID studies, we limited the irradiation time to 100 msec, for which the pressure in the cell is close to the maximum (Laskin, Byrd, & Futrell, 2000; Laskin & Futrell, 2000) as schematically shown in Figure 11. Our experience shows that this gives very reproducible SORI-CID spectra. Provided that SORI waveform is stopped at a right phase, as discussed earlier, extending the SORI waveform beyond this time frame does not result in additional activation of ions. We also

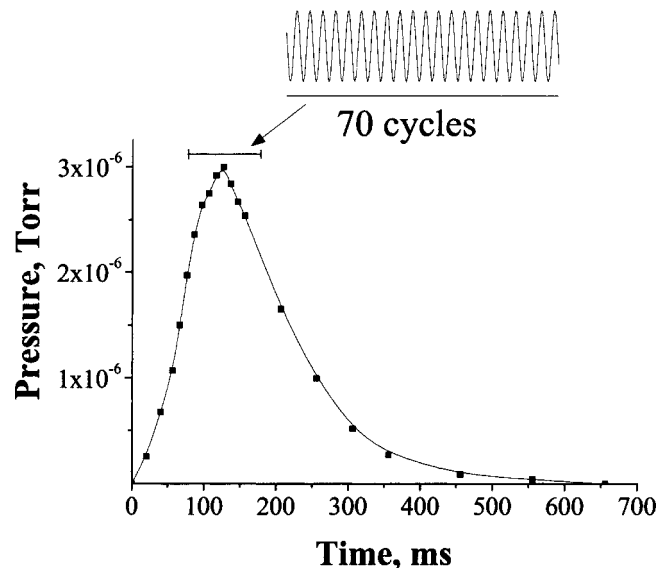


FIGURE 11. Schematic illustration of irradiation time for SORI using pressure profile from Figure 8a.

introduce a delay between the opening of the pulsed valve and switching on SORI waveform. The delay time is determined by the geometry of the vacuum system and the pumping efficiency for a particular collision gas.

3. Offset Frequency and Peak-to-Peak Voltage

The offset frequency (also called beat or difference frequency), $\Delta\omega$, together with the peak-to-peak voltage, V_{p-p} , determine the maximum kinetic energy of the excited ion (E_{lab}^{max}). According to Equation 8, E_{lab}^{max} increases with increase in V_{p-p} and decreases with increase in $\Delta\omega$. Since E_{lab}^{max} determines the maximum CM collision energy it is one of the major factors that affect fragmentation efficiency in MCA-CID. However, these parameters must be chosen carefully because an improper choice can result in distortion of the isotopic distribution of the precursor ion peak and also in unintentional on-resonance excitation and ejection of the fragment ions. Isotopic distortion occurs because the side of the isotopic envelope closest to the excitation frequency has a higher kinetic energy than the side further from the excitation frequency. Increasing the offset frequency can minimize this effect.

The unintentional ejection of fragment ions creates the so-called “blind” spot in the spectrum if the activation frequency is resonant with the reduced cyclotron frequencies of some of the fragment ions. The blind spot is centered at the frequency of the excitation waveform and its width varies with irradiation time and amplitude. The width of the blind spot in the m/z domain decreases at higher cyclotron frequencies (i.e., lower m/z or higher magnetic field strength). For example, in a 7T field a 2-kHz blind spot (0.5 sec irradiation with 8.5 V amplitude) at m/z 1,000 corresponds to 18.6 m/z units, whereas the same 2-kHz blind spot at m/z 500 corresponds to only 4.6 m/z units (Hofstadler

et al., 1994). At 12 T, 2 kHz blind spots at m/z 1,000 and 500 correspond to m/z windows of only 10.9 and 2.8, respectively. Reducing the amplitude of the excitation waveform can significantly reduce the width of the blind spot. This requires adjusting the irradiation time to keep the same level of internal excitation of the precursor ion.

Blind spots can be easily avoided for singly charged ions by applying SORI at a lower frequency—the high mass side of the precursor ion. However, for multiply charged ions, for which reaction products appear on both sides of the precursor ion, the unintentional ejection of product ions presents a serious problem. McLafferty and co-workers gave a remarkable example illustrating this effect (Fig. 12) using SORI-CID of the +17 charge state of the equine myoglobin (Senko, Speir, & McLafferty, 1994). Applying excitation waveform 2 kHz above the cyclotron frequency of the $(M + 17H)^{17+}$ ion produces fragment ions between m/z 1,000 and 1,050 whereas ejecting ions between m/z 950 and 990. SORI excitation at 2 kHz below the cyclotron frequency of the precursor ion shows fragment ions between m/z 950 and 1,000

whereas ejecting ions in the 1,000–1,040 mass range. This requires carrying out two SORI-CID experiments with an excitation frequency above and below the reduced cyclotron frequency of the precursor ion to obtain a complete series of all possible fragment ions for multiply charge precursors.

The efficiency of SORI-CID increases with increase in kinetic energy of the ion. Williams and co-workers studied the effect of $\Delta\omega$ and V_{p-p} on the effective temperature of singly protonated leucine enkephalin and doubly protonated bradykinin (Schnier, Jurchen, & Williams, 1999). This was done by comparing SORI-CID kinetics with kinetics obtained using black-body infrared radiative dissociation (BIRD) and assigning effective temperatures to each SORI-CID kinetic experiment. They demonstrated that the effective temperature (T_{eff}) of the excited ion increases with V_{p-p} and decreases with $\Delta\omega$. T_{eff} depends linearly on $\Delta\omega$, while the dependence on the V_{p-p} is not linear. These experiments were carried out using the same peak pressure in the ICR cell (3×10^{-6} Torr).

As discussed earlier the number of collisions experienced by the ion during SORI increases with kinetic energy of the ion. Figure 13 shows the dependence of T_{eff} on the maximum CM collision energy and the V_{p-p} for a series of small alanine-containing peptides. In these experiments, the same number of collisions at different kinetic energies of ions was maintained by adjusting the peak pressure in the cell as discussed earlier. The data points in Figure 13 were obtained from the average internal energies of excited ions reported elsewhere (Laskin & Futrell, 2002). The effective temperature of the ion increases with collision energy (Fig. 13a). However, at high collision energies it rises more slowly than at low collision energies. This has been attributed to collisional deactivation of ions that becomes increasingly important for hot ions (Laskin, Byrd, & Futrell, 2000; Laskin & Futrell, 2002). The same data plotted against the peak-to-peak voltage (Fig. 13b) shows a linear dependence between V_{p-p} and T_{eff} .

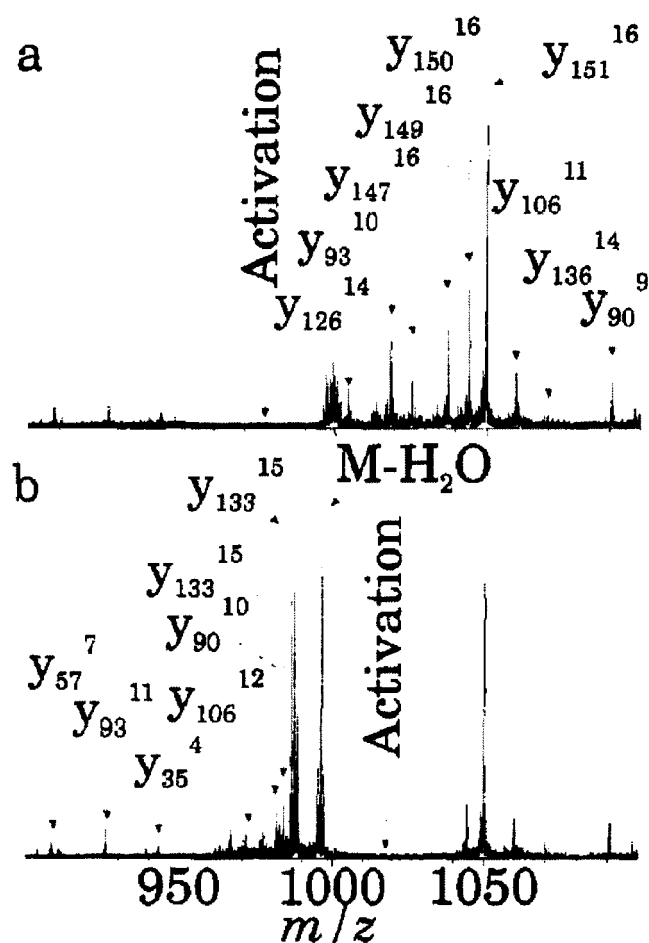


FIGURE 12. SORI MS/MS spectra of $(M + 17H)^{17+}$ from equine myoglobin with activation 2 kHz (a) above and (b) below resonance. Reproduced from Senko, Speir, & McLafferty (1994), with permission from American Chemical Society, copyright 1994.

4. Optimization of Experimental Parameters

Optimization of SORI-CID parameters is important for obtaining efficient fragmentation of ions of interest. A detailed discussion on the efficiency of collisional activation of peptide ions was recently presented (Laskin & Futrell, 2002, 2003a) and will not be discussed in this review. Earlier discussion in this section highlighted some important limitations on the parameters used for the off-resonance excitation. For example, whereas the number of collisions can be increased by increasing the peak pressure and the irradiation time, the maximum pressure in the cell is limited by the capacity and pumping speed of the pumps that evacuate the UHV chamber. The optimum irradiation time is determined by the width of the pressure profile. Both of these limitations can be avoided using multiple pulses of collision gas. In this case, the pressure profile becomes wider and the irradiation time can be increased accordingly. However, this technique requires accurate pressure calibration to optimize the delay time between the successive openings of the pulsed valve. In addition, longer residence time of collision gas in the cell results in ion loss by magnetron expansion of the ion cloud.

For fixed pressure and irradiation time the kinetic energy of ions can be varied by changing V_{p-p} and $\Delta\omega$. As mentioned

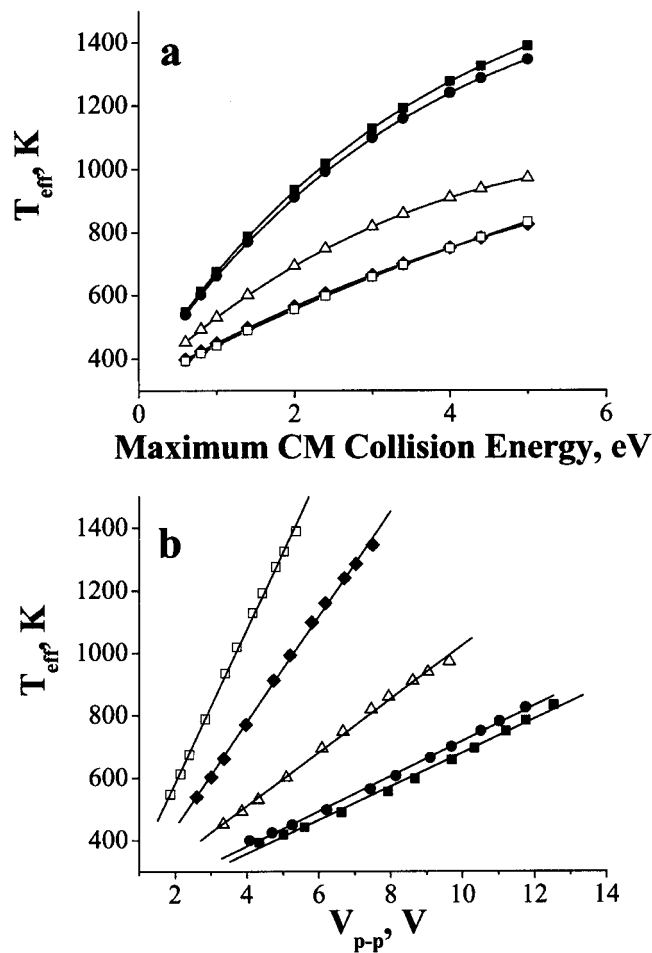


FIGURE 13. The dependence of T_{eff} on (a) the maximum CM collision energy and (b) the V_{p-p} for a series of small alanine-containing peptides.

earlier, the latter parameter should be varied with great caution to avoid isotopic distortion and unintentional ejection of fragment ions from the cell. The situation is much simpler for singly charged ions, for which blind spots are avoided by exciting ions below the cyclotron frequency. However, ions generated by MALDI fall in a very broad m/z range, which makes optimization of SORI-CID parameters time-consuming. This is particularly important when only a small amount of sample is available for each experiment. A technique for optimization of SORI-CID parameters for ions generated by MALDI was recently presented (Mirgorodskaya, O'Connor, & Costello, 2002). The authors found that optimal V_{p-p} is largely independent of m/z if the offset (difference) frequency is kept at 1.5% of the reduced cyclotron frequency of the ion. This method considerably simplified optimization of SORI-CID for analysis of carbohydrates, glycoconjugates, and peptides over the mass range m/z 300–3,500, requiring optimization of only V_{p-p} , and only for the first MS/MS stage. Peak-to-peak voltage close to 20 V was used in this study. It has been demonstrated that when the offset frequency is varied in such a way the CM collision energy is independent of the mass of the ion. However, it is surprising that

similar fragmentation efficiencies were obtained using the same CM collision energy for ions over such a wide mass range, since one expects that dissociation rates strongly depend on the size of the ion. Since the pressure and irradiation time were fixed in these experiments the number of collisions experienced by low-mass ions is higher than the number of collisions experienced by heavier ions. In addition, the offset frequency is larger for smaller ions. This changes the ratio of the beat frequency to the collision frequency, which can cause some damping of the kinetic energy of lighter ions as discussed earlier. Nevertheless the above approach appears to be very useful for identification of ions generated by MALDI.

F. Applications

1. High Mass Accuracy

SORI-CID provides a means for obtaining fragmentation spectra of complex molecules with very high mass accuracy, an important prerequisite for successful application of any ion activation method to structural characterization of large molecules. Heck & Derrick (1997) utilized very precise isolation of the precursor ion prior to SORI-CID for obtaining isotopically “pure” fragmentation patterns. The method was first demonstrated for doubly protonated bradykinin, for which mass accuracy in detection of the fragment ions was on average 1.2 ppm. The method was further extended to study selective fragmentation of single isotopic ions of proteins up to 17 kDa using 9.4 T FT-ICR MS (Heck & Derrick, 1998). However, this type of experiment is quite tedious and introduces certain limitations for application of SORI-CID for peptide and protein identification. In addition, because of the very strict requirements for the isolation of an isotopic peak significant amount of kinetic energy can be deposited into the ion during the isolation event, which is a serious obstacle for studying energetics of isotopically pure precursors.

A more common strategy relies on accurate mass calibration. Because frequency determinations in FT-ICR MS can be significantly affected by differences in ion populations (space-charge effects) between the calibration spectrum and the spectrum of interest as well as drift in the magnetic field strength, ion trapping conditions, and detection parameters, external calibration commonly results in substantial mass errors. Muddiman and co-workers suggested a strategy for accurate mass determination using SORI-CID that utilizes internal calibration (Flora, Hannis, & Muddiman, 2001). The analyte and the calibrant are introduced into the system using a dual electrospray source. This eliminates the potential analyte signal suppression by ionization of the internal standard and makes the choice of the calibrant fairly straightforward. Accurate mass measurements with average mass error ranging from -1.2 to -3.2 ppm for a 15-mer oligonucleotide have been reported.

2. SORI-CID and Ion Axialization

Because of magnetron orbit expansion fragment ions generated using SORI may diffuse radially out of the trap at high pressures of the collision gas. Even if the fragment ions remain in the trap,

their spatial distribution (large magnetron radius) may be quite large, severely limiting mass resolving power and mass accuracy. Marshall and co-workers presented a technique in which quadrupolar axialization is performed either simultaneously (Guan, Marshall, & Wahl, 1994) or immediately after off-resonance excitation. This approach results in significant improvements in FT-ICR detection efficiency, mass resolving power, and mass accuracy. It is particularly useful for SORI-CID experiments in a dual cell, for which ion axialization is critical for efficient transfer of all ions into the analyzer cell for mass analysis.

3. Radial Separation of Mass-Selected Ions

Off-resonance excitation of ion motion can be utilized to remove unwanted ions from the optical path during the photodissociation process (Shin & Han, 1997). These ions can be further returned to the center of the cell for mass analysis. This is a useful technique for mass-selective dissociation of ions by IRMPD. Shin and Han studied photodissociation of isotopomers of bromotoluene and demonstrated that dissociation of a single isotope could be obtained by removing another isotope from the optical path of the laser.

4. In-Trap Cleanup

Because of the gentle nature of electrospray ionization a variety of non-covalent complexes are often formed in the ionization stage. The presence of a variety of non-covalent adducts from impurities in the sample seriously complicates mass spectra and affects both the resolution and sensitivity. For example, adducts containing Na^+ or K^+ are the most common species present in mass spectra. Smith and co-workers presented an in-trap cleanup approach using SORI-CID performed under mild conditions (Tolic et al., 1998). Under these conditions non-covalent complexes are efficiently dissociated without significant dissociation of covalently bonded species. In-trap cleanup of proteins from electrospray ionization yields improved mass accuracy and resolution. A similar approach was used by Little & McLafferty (1996) using IRMPD. In comparison to IRMPD in-trap cleanup using SORI-CID is m/z selective, which is advantageous when the mass of the most dominant adduct (or several adducts) is known.

Another example of the SORI in-trap cleanup was presented for identification of a 49 kDa protein (Maier et al., 2000). The mass spectrum of dialyzed protein showed heavily adducted ions, which prevented the assignment of charge states of the protein. Charge-state assignment was possible only after a gentle SORI cleanup. HPLC purification of the protein combined with the cleanup procedure provided a high-quality mass spectrum.

5. Simultaneous Fragmentation of a Mixture of Ions

Smith and co-workers presented a new approach for identification of peptides and proteins in which the SORI waveform is composed of multiple frequencies (Hofstadler et al., 1994). The multiple-frequency approach takes advantage of the superposition principle, which states that two or more waves traverse

space independently of one another. Consequently multiple frequencies act independently of each other in this variation of the SORI technique. This approach can, therefore, be applied for activating both the precursor ion and its selected fragment, thus providing enhanced sequence information. Irradiating several charge states of the same peptide or protein may also be advantageous to increase the MS/MS signal and improve sequence coverage. However, the limitations of SORI discussed earlier are magnified in multiple-frequency experiments. Each activation frequency creates its respective blind spot. The initial phase effects can result in a large initial beat in the waveform from constructive interference of the frequencies leading to ion loss. Ion losses from this effect can be alleviated using proper apodization of the excitation waveform that prevents any impulse excitation of ions.

6. MS^n

Multiple MS/MS stages are commonly used for structure determinations of complex molecules. MS^n is particularly important for structural analysis of carbohydrates, which is challenging because of diversity of structural isomers characteristic of carbohydrates (Solouki et al., 1998). Multiple stages of MS/MS allow mapping of specific dissociation pathways for selected fragment ions, leading to products that cannot be obtained directly from the precursor ion. In addition, knowing the hierarchy of ion fragmentation can be useful in distinguishing isobaric fragment ions. Non-destructive FT-ICR detection can be utilized to perform multiple remeasurement of the same ion population. This feature, combined with isolation of an ion of interest and ejection of all unwanted ions, constitutes the basis for MS^n experiments in FT-ICR MS. SORI-CID is well suited for MS^n experiments because ion activation leaves ions close to the center of the cell; this is important for efficient ion remeasurement. However, magnetron expansion of the ion cloud can result in substantial ion loss during MS^n experiments. As mentioned earlier, this problem can be alleviated using quadrupolar axialization of the ion cloud.

In 1994, Marshall and co-workers demonstrated four-stage SORI-CID (MS^4) of singly protonated bradykinin ions produced by MALDI (Huang et al., 1994). High mass resolution was achieved in all four MS stages. However, the resolution decreased from 50,000 to 2,500 in proceeding from the first to the fourth MS stage. This was attributed to a smaller number of ions and inefficient trapping of fragment ions after multiple SORI-CID stages. High-resolution and high-sensitivity multistage (up to MS^3) SORI-CID spectra of peptides were obtained for MALDI generated ions (Solouki et al., 1996). In this work, SORI-CID was followed by axialization of fragment ions. It has been demonstrated that SORI-CID can be utilized for structural characterization of trace amounts of biological samples. High mass resolving power of FT-ICR allows identification of isotopically resolved peaks for fragment ions. In this case, fragment ion identification is facilitated by comparison of experimental and calculated isotopic distributions. The number of consecutive MS stages is practically limited by the fragmentation efficiency of SORI-CID and the efficiency of ion remeasurement (Solouki et al., 1996). Greatest efficiency is achieved if only one major fragment ion is formed in each MS stage.

Multiple SORI-CID stages can be used for top-down characterization of proteins. Wu et al. (1995) studied dissociation of the +15 charge state of cytochrome c ions from different sources. SORI-CID results in numerous backbone cleavages of the proteins. Competing dissociation pathways, multiple losses of small molecules from the precursor and fragment ions, multiple charge states originating from a single cleavage site, and peak overlapping increase the complexity of SORI-CID spectra and complicate accurate peak assignments. In this case, multiple MS stages are required for unambiguous identification of a protein. Up to four stages of mass spectrometry (MS^4) have been achieved for cytochrome c variants without the need for quadrupolar excitation/collisional cooling of the fragment ions.

7. Structure Determinations Using SORI-CID

Several recent reviews discussed the application of MS/MS for peptide and protein identification (Burlingame, Boyd, & Gaskell, 1998; Aebersold & Goodlett, 2001; Godovac-Zimmermann & Brown, 2001; Mann, Hendrickson, & Pandey, 2001). In this review, we will discuss only selected studies that demonstrate the utility of SORI-CID for examining structures and relative stabilities of proteins and protein-ligand complexes in the gas phase (Senko, Speir, & McLafferty, 1994; Wu et al., 1995; Liu et al., 1996; Wu et al., 1997; Gao et al., 1999). Fragmentation patterns obtained using SORI-CID are very sensitive to small changes in the primary structure of peptides and proteins. For example, different fragmentation spectra were reported for the +15 charge state of cytochrome c variants as shown in Figure 14 (Wu et al., 1995). Replacing three out of 104 residues of the cytochrome c dramatically changes the dissociation pattern. Numerous examples of the influence of the secondary structure on observed dissociation patterns were given based on the detailed comparison of types of cleavages observed in SORI-CID spectra of cytochrome c variants. Interestingly, it was observed that for all four proteins there was no fragmentation in the region of residue 10–20. The lack of fragmentation between residues 10–20 was attributed to the presence of the heme group, which strongly binds to the polypeptide backbone in this region. Furthermore, the observed fragmentation patterns indicated that all proteins were largely denatured in the gas phase. This study suggested that SORI-CID can be a useful tool to probe not only small differences in the primary sequences of proteins but also for probing their higher-order structures and obtaining information not readily available from H/D exchange or circular dichroism studies.

Liu et al. (1996) studied interactions of bacteriophage T4 regA protein with RNAs of various sizes using SORI-CID. Surprisingly, it was observed that the complex dissociates by breaking covalent bonds of the protein itself rather than decomposing to intact protein and RNA. All major fragment ions originated from the 62 amino acid residues at the N-terminus of the protein. It was suggested that identification of these fragment ions may be potentially used to localize the RNA binding domain in the protein. The underlying assumption is that SORI fragmentation occurs at sites not directly involved in protein-RNA binding. Fragmentation in the protein-RNA binding region is less likely because it requires both cleavage of the protein backbone

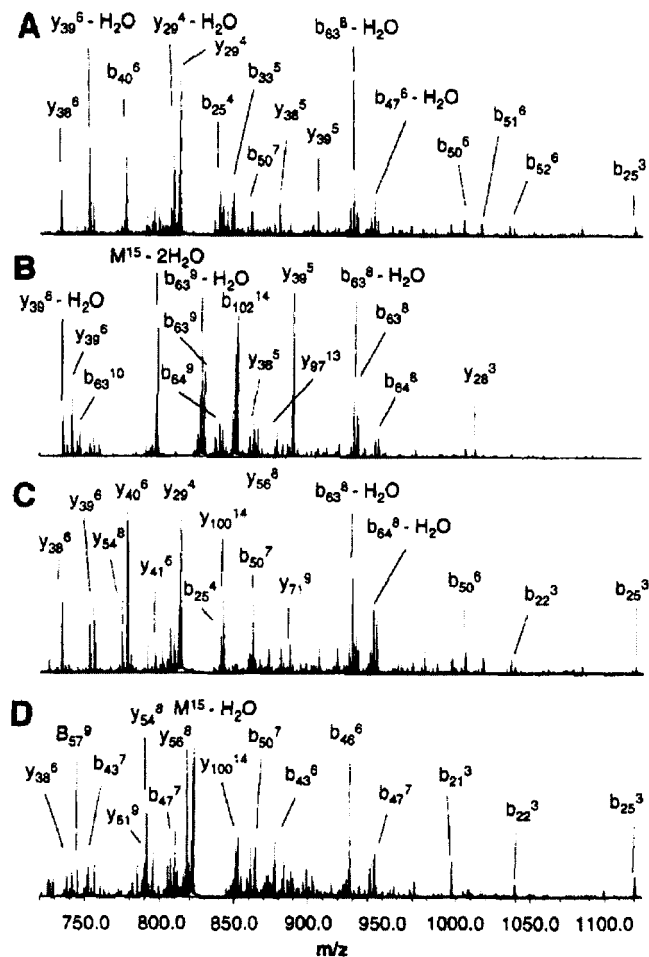


FIGURE 14. SORI-CID spectra ($-1,500$ Hz) of the 15+ charge state ions under identical experimental conditions: (A) bovine cytochrome c; (B) tuna cytochrome c; (C) rabbit cytochrome c; (D) horse cytochrome c. Reproduced from Wu et al. (1995), with permission from American Chemical Society, copyright 1995.

and the electrostatic interaction between the protein and RNA. Gao et al. examined the relative energetics of dissociation of carbonic anhydrase II (CAII)-ligand complexes in the gas phase by determining the excitation voltage resulting in 50% dissociation of the complex (Gao et al., 1999). The higher stability of the CAII complex with benzenesulfonamide in comparison with the complex with apoCAII was attributed to the specific interaction between the ligand and Zn(II) ion on CAII that is present both in solution and in the gas phase.

An interesting example of studying non-covalent interactions in the gas phase was the demonstration by Smith and co-workers that SORI-CID can be used to investigate the binding of metal ions and their complexes to oligonucleotides, providing not only information on the number of metal ions binding to the oligonucleotide, but also information related to the binding site(s) and binding specificity (Wu et al., 1996). CID of the metal complexes with two oligonucleotides, d(pGCTTGCATp) and

d(TTGGCCCTCCTT) revealed that metal ions preferentially bind to the central thymine region of the sequence. The most probable binding sites were the phosphodiester backbone since the sum of the maximum number of charge additions from the metal ions and the charge state of the whole complex was found to be equal to the number of ionizable protons on the DNA backbone. Although site-specific and sequence-specific binding was observed for all three of the metal ions studied, the binding specificity of UO_2^{2+} ions was significantly greater than for Mg^{2+} and Na^+ .

Structural characterization of biological carbohydrates is particularly challenging and requires multiple stages of MS/MS along with the high mass resolving power of FT-ICR for unambiguous identification of fragment ions. Furthermore, sensitivity can be significantly enhanced using multiple ion remeasurement stages (Solouki et al., 1998). Lebrilla and co-workers combined alkaline degradation with MALDI-FTMS analysis to obtain both sequence and linkage information for carbohydrates (Cancilla, Penn, & Lebrilla, 1998). In this case, SORI-CID was used to provide linkage information by inducing cross-ring cleavages. SORI-CID in combination with ion-molecule reactions was utilized for determining phosphorylation sites in carbohydrates (Leavell, Kruppa, & Leary, 2002). Phosphorylated hexoses were reacted with trimethyl borate (TMB) to form complexes. SORI-CID of the hexose phosphate-TMB complex yields diagnostic ions, specific for the phosphate position. These are just a few examples for carbohydrate characterization using SORI-CID. This subject is discussed in detail in an accompanying review in this special issue.

Similar challenges are addressed in studies focused on determination of sequence information from the fragmentation pathways of oligonucleotides (Rodgers et al., 1994; Hettich & Stemmler, 1996; Wu et al., 1996; Flora, Hannis, & Muddiman, 2001; Null & Muddiman, 2001) and peptide nucleic acids (Flora & Muddiman, 2001a). Structural analysis of polymers (Pastor & Wilkins, 1998; Koster et al., 2000) is yet another example from the wide spectrum of applications of SORI-CID.

8. Specific Preparation of Ions Using SORI-CID

The selectivity and specificity of SORI-CID allows preparation of a variety of ions that cannot be prepared using other methods. Guo & Grutzmacher (2000) prepared a number of carbon cluster ions of the form C_nH_x^+ ($n = 18, 20, 24$; $x = 4-12$) by consecutive elimination of hydrogen atoms from polycyclic aromatic hydrocarbons (PAHs) and studied their gas-phase reactions with dimethyl disulfide (DMDS). The reactivity and structure of carbon cluster ions depends on the structure of the PAH from which the ion was prepared. It follows that these ions do not isomerize to a common structure following SORI-CID, another confirmation of the soft nature of this activation technique. Trends in the reactivity of these clusters suggest that they have graphitic structures separated from their more stable isomers by a substantial barrier.

Nelson & Kenttamaa (2001) prepared a doubly aromatic 3,5-didehydrophenyl cation via SORI-CID of 3,5-dinitrobenzoyl chloride. The structure of the ion was determined by comparison of the ion-molecule reactivity of this ion with reactivity of its cyclic and acyclic isomers. It has been shown that the soft nature of SORI-CID allows preparation of this ion in good purity, which

is not possible using electron impact ionization (EI). Specifically, 3,5-didehydrophenyl ions generated by EI readily isomerize into their acyclic and other cyclic counterparts.

9. Fragmentation Energetics of Large Ions from SORI-CID Data

Fragmentation energetics of large molecules can be explored qualitatively by comparing the relative kinetic energies required to induce ion dissociation. Cancilla et al. (1999) studied the effect of the coordinating alkali metal on dissociation energetics of oligosaccharides by comparing multiple-collision dissociation thresholds (MCDT) for different fragmentation pathways. It has been demonstrated that glycosidic bond cleavages are likely to be charge-induced processes, which is manifested by differences in MCDTs for different coordinating metal ions. Li^+ -coordinated oligosaccharides have the lowest activation barrier for glycosidic bond cleavages. In contrast, MCDTs for cross-ring cleavages are independent of the alkali metal.

Quantitative fragmentation energetics can be extracted from energy-dependent SORI-CID data using RRKM modeling (Laskin, Byrd, & Futrell, 2000; Laskin & Futrell, 2000). This approach has been recently reviewed (Laskin & Futrell, 2003a) and will be discussed here only briefly. SORI-CID experiments are carried out at several collision energies. Relative intensities of ions in MS/MS mass spectra are plotted as a function of collision energy to generate fragmentation efficiency curves (FECs). These are modeled using RRKM theory for dissociation rate constants and a newly developed analytical function for the internal energy distribution (IED) of excited ions.

This approach was initially tested by studying fragmentation energetics of bromobenzene (Laskin, Byrd, & Futrell, 2000) and 1-bromonaphthalene (Laskin & Futrell, 2000) radical cations, for which fragmentation energetics are well established. It was later applied to fragmentation of small alanine-containing peptide ions (Laskin, Denisov, & Futrell, 2000; Laskin, Denisov, & Futrell, 2002; Laskin, Bailey, & Futrell, 2003; Bailey, Laskin, & Futrell, 2003). Total decay of the precursor ion and buildup of different fragment ions was utilized to study fragmentation energetics of these peptides in great detail. Dissociation energies for the major reaction channels for polyalanines decrease with increasing peptide size. However, it has been realized that because SORI-CID is a slow activation method it can result in serious discrimination against dissociation fragments formed via competitive reaction channels (Laskin, Denisov, & Futrell, 2001). When the lowest-energy channel opens up, dissociation efficiency through the higher-energy channel is determined by the rate of ion activation. If activation is slow compared to dissociation through the low-energy pathway, the fragment corresponding to the higher-energy pathway is strongly suppressed. For this reason, extracting fragmentation energetics from SORI-CID data should be done with great caution.

III. MULTIPHOTON DISSOCIATION

Photoexcitation of ions can be effected using both pulsed infrared (IR) or ultraviolet/visible (UV/vis) and continuous (CW) infrared

laser irradiation. Absorption of UV/vis photons by ions occurs by resonant photon absorption from the ground to an excited electronic state and commonly results in photodissociation of the excited ion. Photodissociation of peptides and small proteins has been achieved using 193 nm (6.42 eV) photons (Bowers et al., 1984; Bowers, Delbert, & McIver, 1986; Williams, Furlong, & McLafferty, 1990; Beu et al., 1993). However, photodissociation of larger proteins (ubiquitin ions, 8.6 kDa) resulted in formation of small, uninformative fragment ions (Beu et al., 1993). Ultraviolet photodissociation of small ions has been extensively reviewed (Berkowitz, 1979; Dunbar, 1984, 2000; Vanderhart, 1989, 1992) and will not be further discussed in this review.

Excitation using IR lasers relies on vibrational transitions resulting from photon absorption. Because the spacing between vibrational states is much smaller than the spacing between electronic states the mechanism of IR excitation of the ion can be quite different. High-power pulsed IR irradiation was particularly useful for studying multiphoton dissociation of small molecules. Excitation of small molecules usually requires resonant absorption of several IR photons followed by incoherent excitation (Lupo & Quack, 1987). In this case, resonant absorption is the rate-limiting step and presents a “bottleneck” for the IR excitation. As a result, excitation of small molecules by IR radiation requires high-power lasers. The system reaches the quasi-continuum of vibrational states when the density of states becomes large enough such that there is at least one vibrational state within the laser bandwidth. In the quasi-continuum excitation readily occurs by incoherent absorption of multiple IR photons (Bomse, Woodin, & Beauchamp, 1979 and references therein).

Beauchamp and co-workers were the first to demonstrate the utility of low-intensity CW infrared radiation for multiphoton dissociation of gas phase ions (Woodin, Bomse, & Beauchamp, 1978; Bomse, Woodin, & Beauchamp, 1979). In particular, they studied decomposition of the protonated diethyl ether and its proton-bound dimer. They found that multiphoton excitation resulted in facile decomposition of the dimer, whereas dissociation of protonated diethyl ether required considerably higher laser power. Estimation of the densities of vibrational states demonstrated that for the dimer the quasi-continuum is reached by absorption of only one photon whereas absorption of four photons is necessary to access the quasi-continuum for the monomer. Infrared multiphoton dissociation (IRMPD) of small polyatomic ions with low-power CW lasers has been studied by a number of groups (Bomse & Beauchamp, 1981a,b; Bomse, Berman, & Beauchamp, 1981; Jasinski et al., 1982; Tumas et al., 1983; Baykut et al., 1985; Shin & Beauchamp, 1990; Dunbar, 1991; Uechi & Dunbar, 1992; Dunbar & Zaniewski, 1992; Huang & Freiser, 1993). Early studies have been reviewed by Thorne & Beauchamp (1984).

Based on the above discussion, it is clear that large molecules should have a quasi-continuum of vibrational states at room temperature, making them an ideal target for IRMPD. Eyler and co-workers first demonstrated IRMPD of relatively large ions produced by laser desorption with m/z values in the range 400–1,500 (Watson, Baykut, & Eyler, 1987). McLafferty and co-workers demonstrated the utility of IRMPD for efficient fragmentation of multiply charged ions from proteins and

oligonucleotides (Little et al., 1994). Since then low-power cw IRMPD has been widely used for structural characterization of large biologically relevant molecules in FT-ICR MS.

A. Fundamental Principles of IRMPD of Large Ions

1. Internal Energy Distribution

In the absence of dissociation the IED of ions excited with low-intensity cw infrared radiation is well approximated by a Boltzmann distribution (Dunbar, 1991). The slow nature of ion excitation allows for efficient competition between the absorption and emission of IR photons. Because IR excitation of large ions is completely incoherent, the rate of absorption and spontaneous/stimulated emission can be readily evaluated using Einstein coefficients. It follows from these considerations that, although the nature of the single-photon IR excitation is quite different from blackbody infrared heating, the net effect of the two excitation techniques is the same: thermalization of ion's vibrational degrees of freedom. In this review, we limit our discussion to the most essential points for understanding the IRMPD data.

When dissociation of excited ions is slow compared to photon absorption/emission ion dissociation is in the so-called rapid exchange limit (REX), for which it can be assumed that in every instance the IED of excited ions is given by a Boltzmann distribution. If ion dissociation is fast relative to ion activation the thermal distribution is depleted. Similarly to BIRD depletion of the thermal distribution by IRMPD has been modeled using master equation modeling (Dunbar, 1991; Uechi & Dunbar, 1992; Dunbar & Zaniewski, 1992; Jockusch, Paech, & Williams, 2000; Freitas, Hendrickson, & Marshall, 2000; Paech, Jockusch, & Williams, 2002). In master equation modeling, the entire internal energy range is divided in small bins. Each bin is populated by photon absorption and depopulated by photon emission and dissociation. Rates of photon excitation/de-excitation are calculated from the corresponding Einstein coefficients. Dissociation rates are calculated using RRKM theory. Figure 15 (Dunbar, 1991) shows a random walk simulation of the temperature of laser-excited ions in the absence of dissociation. There is an excellent agreement between master equation modeling (open symbols) and the blackbody curve (line). There is a slight deviation between the actual IED for (Ala-Gly)₈ ions excited by cw laser (dashed line) and blackbody irradiation (solid line) as shown in Figure 16 (Freitas, Hendrickson, & Marshall, 2000).

Time evolution of the IED of protonated leucine enkephalin during continuous laser irradiation (24.1 W CO₂ laser) is shown in Figure 17a (Jockusch, Paech, & Williams, 2000). The ions are heated up without dissociation for the first 0.4 sec. During this time the IED becomes wider and shifts towards higher energies. After 0.4 sec, the shape of the distribution remains almost the same, while the entire ion population is depleted by dissociation. The snapshot taken at 0.5 sec (Fig. 17b) shows that the IED of leucine enkephalin is narrower than the Boltzmann distribution representing the same most probable internal energy of excited ions. This indicates that in this case dissociation is not occurring in the REX limit.

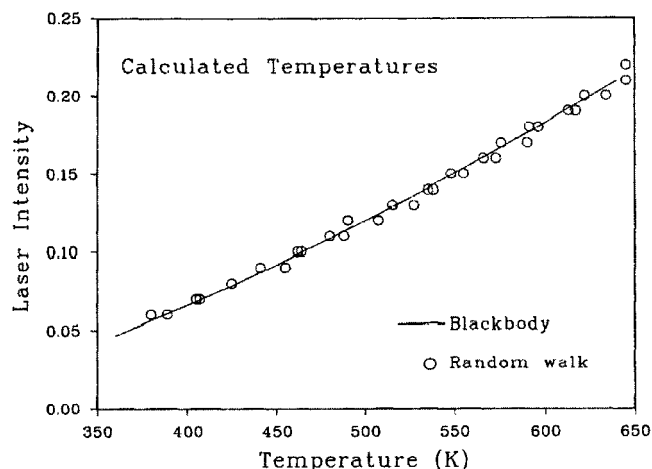


FIGURE 15. The relation between laser intensity and population temperature in the absence of the dissociation reaction, assuming the conditions for the black-body equivalence are met as discussed in the text. The solid line is the black-body curve from Figure 1 and the circles are the points generated by the random-walk simulation. (The units of laser intensity are arbitrary). Reproduced from Dunbar (1991), with permission from American Physical Society, copyright 1991.

2. Temperature of Laser-Excited Ions

Dunbar (1991) demonstrated for a population of ions that absorb and emit radiation only at the laser frequency the temperature of

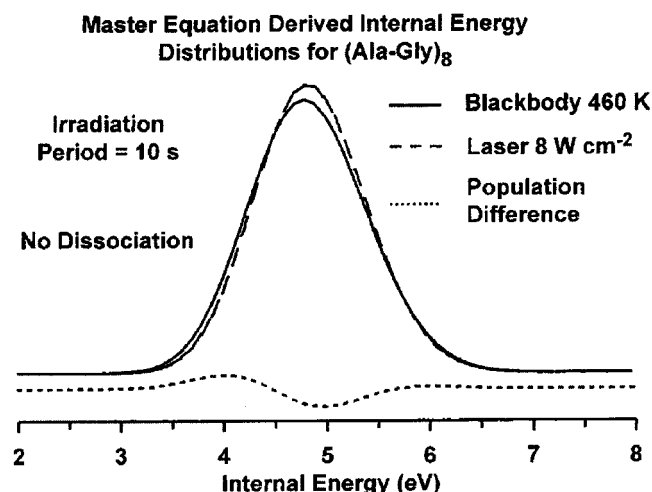


FIGURE 16. Master equation-calculated internal energy distributions (IEDs) for a non-dissociating population of (AlaGly)₈ irradiated by either a 460 K blackbody (solid line) or a 8 W cm⁻² CW CO₂ laser (dashed line). The IED from 8 W cm⁻² CO₂ laser irradiation very closely resembles that from blackbody IR irradiation. Reproduced from Freitas, Hendrickson, & Marshall (2000), with permission from American Chemical Society, copyright 2000.

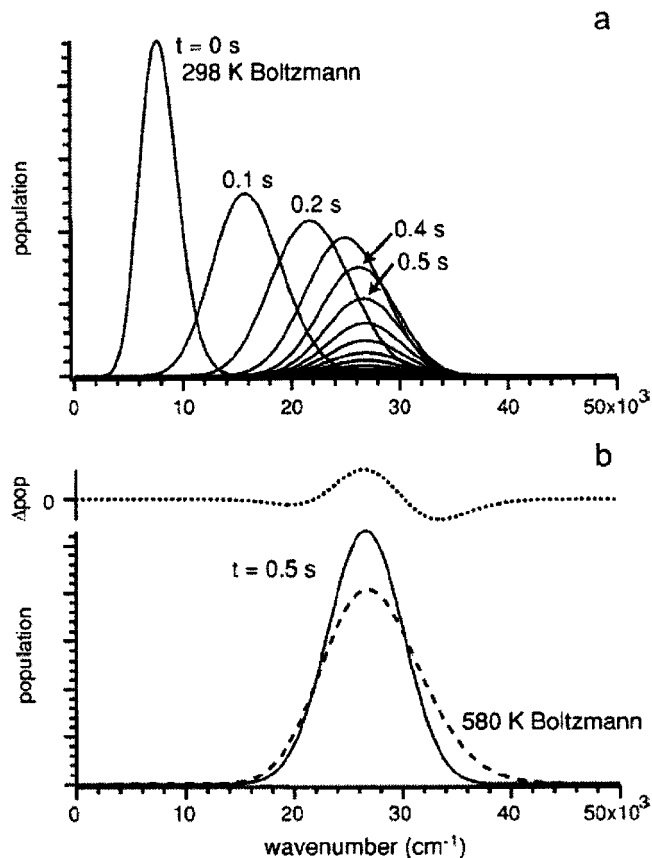


FIGURE 17. Calculated ion IED of LeuEnk•H⁺ at 24.1 W laser power. **Part a** follows the time evolution of the distribution in 0.1 sec time steps. **Part b** compares the steady-state energy distribution (solid line) to a Boltzmann distribution at 580 K (dashed line). Both curves are normalized to the same area. The difference between these distributions (dotted line) is shown separately. Reproduced from Jockusch, Paech, & Williams (2000), with permission from American Chemical Society, copyright 2000.

the population, T , is related to the laser intensity, $I(h\nu)$, via the Planck relation:

$$I(h\nu) = \frac{I(h\nu_0)}{\exp(h\nu/k_B T) - 1} \quad (10)$$

where h and k_B are Planck's and Boltzmann constants, respectively. The temperature increases with increase in the laser intensity (see Fig. 15). An important property of low-intensity IR heating is that the temperature does not depend on the radiative strength of the IR transition of the ion. A similar relationship is obtained when all vibrational modes participate in absorption/emission of radiation (Paech, Jockusch, & Williams, 2002). However, in this case, the temperature-intensity relationship is dependent on the properties of the ion. Master equation simulations of the temperature of excited ions for four different peptides using semi empirical (AM1) vibrational frequencies and transition dipole moments are shown in Figure 18. There is a clear

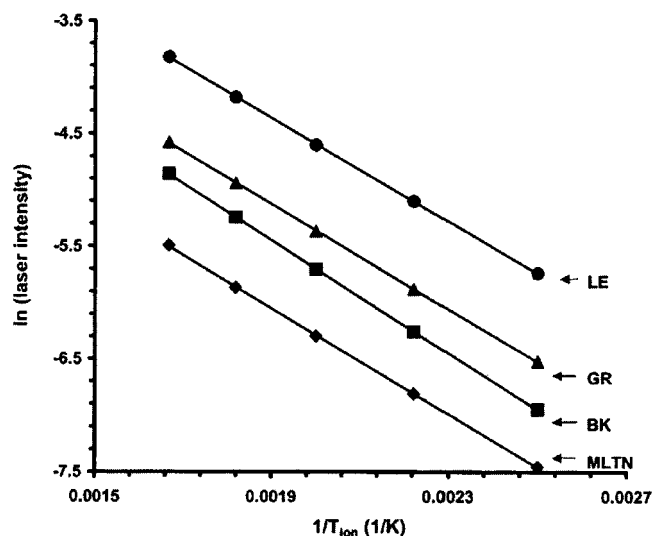


FIGURE 18. Calculated relationship between the relative laser intensity and the ion internal temperature based on AM1-generated frequencies and intensities for four peptides: LE (triangles, leucine enkephalin), GRS (squares, gramicidin S), BK (diamonds, bradykinin), and MLTN (circles, melittin). Reproduced from Paech, Jockusch, & Williams (2002), with permission from American Chemical Society, copyright 2002.

linear relationship between the logarithm of the laser intensity and the reciprocal of the temperature ($1/T$):

$$\frac{d \ln I(h\nu)}{d(1/T)} = -s. \quad (11)$$

In the simplest case, when ion absorbs and emits radiation only at the laser frequency $s = qh\nu$ (see Eq. 10), where q is the partition function for the mode that absorbs radiation. For irradiation with a CO_2 laser at 943.4 cm^{-1} q is between 1.01 and 1.1. For a more complex situation, when all vibrational modes contribute to photon absorption/emission the proportionality constant, s , depends on relative intensities of vibrational transitions of the excited ion. It follows that for similar compounds, such as peptides and proteins, for which the number of vibrations varies with size whereas their relative absorption intensities do not change significantly, s is expected to remain the same (Paech, Jockusch, & Williams, 2002). In fact, the values of s for the four peptides shown in Figure 18 deviate from each other by less than 9%.

3. Induction Time

It follows from Figure 17b that after the laser is turned on there is first an induction time during which no dissociation occurs. This time is required to heat the ion population from room temperature to the temperature at which dissociation starts. The induction time decreases rapidly with laser power (Uechi & Dunbar, 1992). Figure 19 shows a typical kinetic plot obtained using IRMPD. An induction period of approximately 0.4 sec is followed by a rapid decrease in the relative abundance of the excited ion and the formation of fragments. The induction time is shorter for ions that require lower temperatures for dissociation, i.e., ions with lower

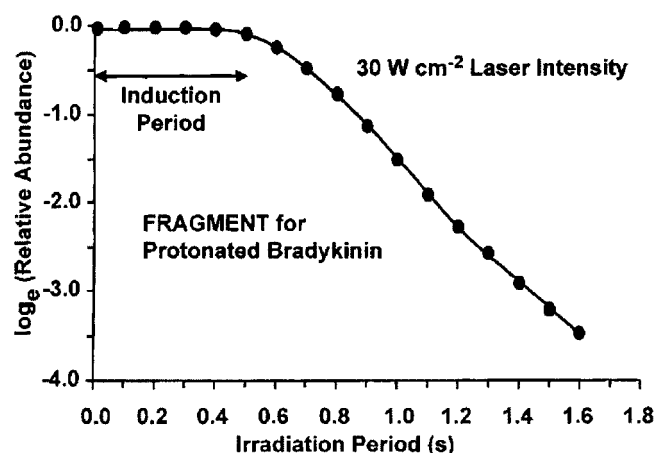


FIGURE 19. Plot of the natural logarithm of precursor ion relative abundance versus time for the dissociation of protonated bradykinin during 30 W cm^{-2} CO_2 laser irradiation. Note the induction time required before the ions gain sufficiently high internal energy to initiate dissociation, after which first-order decay in population is observed. Reproduced from Freitas, Hendrickson, & Marshall (2000), with permission from American Chemical Society, copyright 2000.

dissociation thresholds. Indeed, in most cases the induction delay for peptide ions is around 0.5 sec, whereas only 10–450 msec are required to achieve high-quality IRMPD spectra of large oligonucleotides (Little et al., 1996). The induction time is also affected by the strengths of optical transitions; for example, faster equilibration occurs for ions that have larger transition dipole moments.

4. Kinetics of IRMPD

After the induction time IRMPD follows first-order kinetics. Williams and co-workers demonstrated that the measured dissociation rate depends on total laser power and is rather independent of the diameter of the laser beam (Jockusch, Paech, & Williams, 2000). A simple relationship between the dissociation rate and the laser intensity can be derived from Equation 11:

$$E_a^{\text{laser}} = -k_B \frac{d(\ln k_{\text{diss}})}{d(1/T)} = s k_B \frac{d(\ln k_{\text{diss}})}{d \ln I(h\nu)}, \quad (12)$$

where k_{diss} is the IRMPD rate constant, and E_a^{laser} is the activation energy derived from the IRMPD Arrhenius plot. From Equation 12, it is clear that $\ln(k_{\text{diss}})$ depends linearly on the logarithm of the laser intensity. This relationship holds only for ions that dissociate in the REX limit. For ions that are not in the REX limit the plot of $\ln(k_{\text{diss}})$ versus $\ln I(h\nu)$ deviates from linearity. An example of such deviation observed for the IRMPD of leucine enkephalin is given in Figure 20. The plot also shows the reproducibility of the IRMPD kinetic data.

As mentioned earlier the value of s in Equation 12 is expected to be roughly independent on the size of the ion for a particular class of molecules. Williams and co-workers

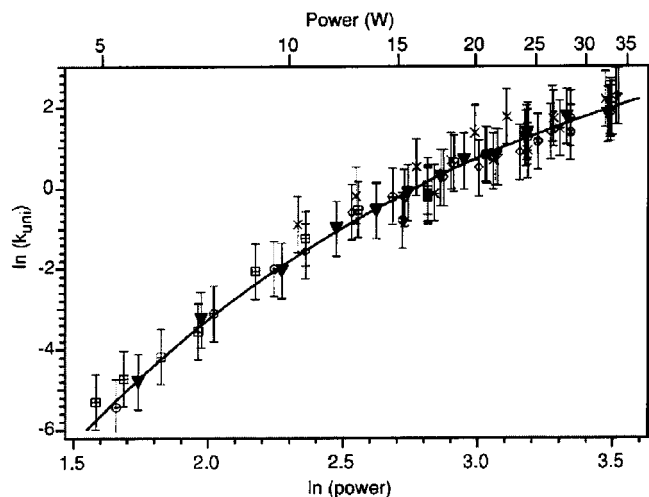


FIGURE 20. Laser photodissociation data for LeuEnk•H⁺ measured over a period of several months. The line is an exponential fit to the data. The error bars are a range of a factor of 2 of the experimentally measured rate constant. Reproduced from Jockusch, Paech, & Williams (2000), with permission from American Chemical Society, copyright 2000.

suggested the following empirical Arrhenius-type relationship for peptides and proteins (Paech, Jockusch, & Williams, 2002):

$$\frac{d(\ln k_{\text{diss}})}{d \ln I(h\nu)} = 4.34 E_a^{\text{laser}}. \quad (13)$$

Arrhenius activation energies can be obtained from Equations 12 and 13 using the following expression (Dunbar, 1991):

$$E_a^{\text{laser}} = E_a + \text{laser pumping correction} + \text{reactive depletion correction}. \quad (14)$$

The laser pumping correction is given by $(q - 1)h\nu \cong 0.1 h\nu$. This correction is small and readily estimated. The reactive depletion correction is important when dissociation is not in the REX limit. The explicit expression for the reactive depletion correction can be found elsewhere (Dunbar, 1991, Equation 17). This correction decreases rapidly with increase in the size of the molecule and is expected to be negligibly small for large molecules. For example, Marshall and co-workers found that for (AlaGly)₈H⁺ there is an almost perfect overlap between the IEDs of ions with and without dissociation (Freitas, Hendrickson, & Marshall, 2000), implying that the reactive depletion correction for this size system is close to zero. The corresponding correction for excited n-butylbenzene ions is 0.05 eV (Uechi & Dunbar, 1992).

5. Experimental Parameters That Affect the Efficiency of IRMPD

IRMPD dissociation efficiency, defined as the relative abundance of the precursor ion in the IRMPD mass spectrum, depends on the

number of ions irradiated by the laser, the laser intensity and irradiation time. It was mentioned earlier that the dissociation rate constant does not depend on the diameter of the laser beam. However, the total number of ions irradiated by the laser depends on both the beam diameter and the overlap between the laser beam and the ion cloud. It is common practice to use an unfocused laser beam for IRMPD experiments to ensure good overlap with the ion cloud in the ICR cell. However, even with an unfocused laser beam it is not always easy to achieve a good overlap if ions acquired sufficiently large magnetron radius during the trapping or isolation event. Hofstadler, Sannes-Lowery, & Griffey (2001) gave an example of very poor IRMPD for oligonucleotides trapped using sidekick trapping. They concluded that ion ensemble was “parked” on a stable trajectory with a substantial magnetron radius, processing about the central axis of the ICR cell, and that these ions were not in the path of the laser beam. They demonstrated that IRMPD efficiency could be increased dramatically by applying an rf-tickle pulse to excite the cyclotron motion of the ions and improve overlap with the laser beam.

An important property of IRMPD is that it produces fragment ions on the optical axis of the cell. While the laser beam is on, fragment ions can absorb additional IR photons and fragment further. Optimal irradiation time is determined by the interplay between the amount of primary and secondary dissociation in the mass spectrum. Secondary fragmentation can be advantageous because it produces fragments that cannot be obtained directly from the precursor ion. However, it also results in depletion of the amount of primary fragment ions and results in some loss of sequence information. Laser power has a similar effect on the IRMPD spectrum.

B. Comparison of Major Features of SORI-CID and IRMPD

In many cases, SORI-CID and IRMPD produce comparable MS/MS spectra (Surya et al., 1996). Similarity between these two techniques results from the similar nature of ion activation: both methods involve slow heating of ions (internal energy is deposited in small steps) and deposit quasi-thermal distributions of internal energies. In both cases dissociation of excited ions predominantly follows the lowest-energy pathways. Higher-energy competing reaction channels are strongly discriminated when absorption of additional internal energy required for opening the higher-energy pathway competes with dissociation via the low-energy reaction channel. Since IRMPD is more discriminative against higher-energy reaction pathways (Tonner & McMahon, 1997) than SORI-CID it follows that average energy deposition in each step is smaller for IRMPD. For example, Tonner and McMahon found that photodissociation of protonated ethanol produces exclusively the lowest energy fragment ion (H₃O⁺). The threshold energy for the formation of the higher-energy fragment (C₂H₅⁺) differs by only 5 kcal/mol (about twice the photon energy for CO₂ laser, 2.7 kcal/mol, or 0.12 eV). Low-energy CID of the same ion produces a mixture of C₂H₅⁺ and H₃O⁺ in the ratio of 1.3:1.

McLafferty and co-workers compared SORI-CID and IRMPD spectra for several proteins and oligonucleotides and

found that in general both methods produced the same sequence peaks, while their relative abundances could be significantly different (Little et al., 1994). They found that for all charge states of ubiquitin ions SORI gave primarily large b and y ions with a very little fraction of internal fragments. IRMPD gave many more y, b, and internal fragments and significantly smaller amount of fragments corresponding to H₂O loss from b and y ions.

An important intrinsic property of IRMPD is that it is not mass-selective: all ions that are in the optical path of the laser beam are excited simultaneously. This can be advantageous for sequencing large ions produced by electrospray with a distribution of charge states. Similarly to SORI-CID, IRMPD spectra for different charge states can be quite different. In general, fragmentation of lower charge states of proteins require longer irradiation times (Little et al., 1994). For example, for irradiation time sufficient for complete decomposition of the +10, +11, and +12 charge states of ubiquitin, the +7 and +8 charge states remain intact. Simultaneous irradiation of different charge states produces rich MS/MS spectra that contain both intact precursor ions (lower charge states) and sequence specific fragment ions originating from higher charge state precursors. IRMPD can be performed in a mass-selective manner either using a standard ion isolation step or by removing all ions from the optical path of the laser beam and using an rf tickle pulse that brings only ions of interest into the beam (Hofstadler, Sannes-Lowery, & Griffey, 2001).

The lack of mass selectivity also presents a disadvantage of IRMPD. Primary fragment ions can further absorb IR photons and produce secondary fragments. Secondary fragmentation is an important consideration for choosing the irradiation time. As discussed earlier IRMPD efficiency increases with irradiation time. However, longer irradiation results in dissociation of primary sequence-specific fragment ions and loss of sequence information. However, secondary fragmentation can be minimized by removal of the primary fragments from the laser beam soon after their formation (Little et al., 1994). This can be done using SWIFT excitation of all ions except the precursor ion to cyclotron orbits out of the path of the laser beam. McLafferty and co-workers found that to avoid ion ejection from the cell SWIFT excitation should be done periodically during the laser irradiation.

Because photodissociation does not remove ions from the center of the cell and does not involve any rf excitation ion loss is substantially reduced in IRMPD experiments. IRMPD does not disturb isotopic peaks and does not produce “blind spots” in MS/MS spectra—particularly important for sequencing and accurate mass measurements of multiply charged ions. As discussed earlier, because of the “blind spots” two SORI-CID experiments are required to obtain a complete dissociation pattern of multiply charged ions, whereas IRMPD results in a complete fragmentation pattern in only one experiment. Another important advantage of IRMPD over SORI-CID is that the former does not require any gas load, eliminating the lengthy pump down delay and making IRMPD a preferred method for high throughput experiments.

A drawback of IRMPD is that it requires good overlap between the laser beam and the ion cloud. This can be particularly challenging for ions following a large magnetron orbit (see “Experimental Parameters That Affect the Efficiency of IRMPD”). SORI-CID is a more robust method of ion activation

that is largely insensitive to the initial position of the ion cloud in the ICR cell.

C. Applications

In many cases, IRMPD applications mirror the applications of SORI-CID described earlier. These include IRMPD in-trap cleanup (Little & McLafferty, 1996); MSⁿ experiments (Little et al., 1994; Tonner & McMahon, 1997); IRMPD in an external ion reservoir (Hofstadler, Sannes-Lowery, & Griffey, 1999). Because IRMPD does not perturb the ion cloud high mass accuracy and resolution are readily obtained using this technique in combination with internal mass calibration (Dufresne, Wood, & Hendrickson, 1998; Hofstadler et al., 1998; Shi et al., 1999; Kruppa et al., 2002). Hofstadler et al. (1998) utilized the observation that irradiation times for oligonucleotides are five to ten times shorter than for peptides and proteins and used proteins as internal standards for internal calibration of IRMPD spectra of oligonucleotides. They demonstrated for this example that relatively short irradiation pulses result in facile fragmentation of oligonucleotides whereas leaving proteins intact.

1. Structure Characterization Using IRMPD

Application of IRMPD for structural analysis of small molecules is based on isomer differentiation (Bomse & Beauchamp, 1981a; Baykut et al., 1985). Isomer differentiation is possible because photodissociation proceeds via the lowest energy pathway and different isomeric species are likely to have different lowest-energy reaction channels. However, if the isomerization barrier that separates different species is lower than a dissociation barrier for one of the isomers isomer-specific fragmentation is lost because of inter-conversion between different species prior to dissociation. It should be noted that potential energy surfaces of large, biologically relevant molecules are very complex and generally have a large number of low isomerization barriers separating different families of conformers. Consequently dissociation of large molecules necessarily involves a complex mixture of different isomers and it is usually impossible to reach the same level of detail for large molecules obtained in early studies on structures of small molecules.

Similarly to SORI-CID, IRMPD has been utilized for structural characterization and identification of peptides (Li et al., 2001; van der Rest et al., 2001), proteins (Little et al., 1994; Dufresne, Wood, & Hendrickson, 1998), oligonucleotides (Little et al., 1994, 1996; Null & Muddiman, 2001; Hannis & Muddiman, 2002), phosphorylated (Flora & Muddiman, 2001b), and glycosylated peptides (Hakansson et al., 2001), oligosaccharides (Shi et al., 1999; Xie, Schubothe, & Lebrilla, 2003), protein complexes (Kruppa et al., 2002; Yamada, Suzuki, & Hirayama, 2002) as well as characterization of protein conformations (McLafferty et al., 1998).

2. Characterization of Complex Mixtures

For the reasons noted above IRMPD is intrinsically better suited for simultaneous fragmentation of a mixture of ions than SORI-CID. Identification of peptides from IRMPD of complex

mixtures has been demonstrated (Masselon et al., 2000). Both SORI-CID and IRMPD were utilized in data dependent multiplexed MS/MS of protein digests (Li et al., 2001). However, in this case, IRMPD implementation is significantly simpler than SORI-CID. Multiplexed SORI-CID requires a waveform with multiple irradiation frequencies. These are obtained from the initial MS scan, whereas IRMPD activates all ions entering the ICR cell. Because of its non-selective nature IRMPD it is much more easily combined with on-line separations. Marshall and co-workers demonstrated rapid identification of proteins in mixtures using a combination of liquid chromatography, electrospray ionization and IRMPD of protein ions (Li et al., 1999). They suggested that this method is suitable for identification of a mixture of 30–50 proteins.

3. Activation Energies for Dissociation of Large Ions From IRMPD

From the discussion of kinetics of IRMPD presented earlier it is straightforward to describe a strategy for obtaining energetics of dissociation of large molecules using IRMPD data. Dissociation rates can be determined by monitoring the relative intensity of the precursor ion as a function of irradiation time at a particular laser intensity. Activation energy (E_a^{laser}) is obtained from the plot of the logarithm of dissociation rate constant versus logarithm of laser intensity using Equation 13. Arrhenius activation energy is then calculated from E_a^{laser} using Equation 14. This approach was originally derived by Dunbar (1991) and later refined by Williams and co-workers (Paech, Jockusch, & Williams, 2002). It can be used for any sufficiently large (slowly decaying) molecule that dissociates in the REX limit. For smaller molecules, the Arrhenius plot of $\ln(k_{\text{diss}})$ versus $\ln I(h\nu)$ does not give a straight line. In this case, determination of the Arrhenius activation energy requires accurate dissociative master equation modeling, which is quite tedious (Dunbar, 1991; Uechi & Dunbar, 1992; Dunbar & Zaniewski, 1992; Jockusch, Paech, & Williams, 2000).

Most studies of the energetics of dissociation of large molecules utilized the simple approach (Dunbar, 1991) which underestimates the activation energy by approximately 40%. In all cases, the authors limited their studies to determination of relative fragmentation energetics. Absolute activation energies for a number of peptides and small proteins (Freitas, Hendrickson, & Marshall, 1999, 2000; Paech, Jockusch, & Williams, 2002) were re-evaluated by Williams and co-workers using Equation 13. These values are in good agreement with previously published BIRD data (Paech, Jockusch, & Williams, 2002). The only exemption is singly protonated bradykinin, for which the activation energy obtained from IRMPD (1.94 eV) is substantially higher than that obtained from BIRD experiments (1.3 eV). The reason for this discrepancy is not clear. Muddiman and co-workers applied a similar technique to obtain relative energetics of oligonucleotides and their modified (7-deaza purine) analogs (Hannis & Muddiman, 2002) as well as phosphorylated peptides (Flora & Muddiman, 2002). They confirmed that phosphorylation lowers the activation energy for total decomposition of peptide ions.

The advantage of using IRMPD as compared to BIRD for such studies is twofold. Firstly, laser heating allows easy access to substantially higher temperatures than physical heating of the

ICR chamber utilized in BIRD experiments. Consequently, molecules that are stable at the highest temperatures accessible in BIRD experiments can be readily dissociated using IRMPD. Secondly, a lengthy thermal equilibration of the ICR chamber prior to BIRD experiments is eliminated in IRMPD studies, enabling rapid acquisition of thermal data.

An important limitation of the IRMPD thermal kinetics is that information on the Arrhenius pre-exponential factor, A , is lost. This can be understood by examining Figure 18. The actual temperature to which the system is heated depends on the molecule. Replacing $\ln(1/T)$ with $\ln I(h\nu)$ in Equation 12 is possible because plots of $\ln I(h\nu)$ versus $\ln(1/T)$ have the same slope. However, this substitution loses the information on the intercept of the Arrhenius plot, i.e., $\ln A$. This is a very important limitation of the method because it has been demonstrated that even when Arrhenius activation energies are correctly extracted from the data they do not necessarily represent actual dissociation energies even in a relative sense (Laskin & Futrell, 2003c). Arrhenius activation energy (E_a) represents an average over the entire ensemble of activated species. It can be converted into the dissociation threshold (E_0) using Tolman's theorem (Gilbert & Smith, 1990; Dunbar, 1991; Baer & Hase, 1996):

$$E_a = E_0 + \langle E' \rangle(T) - \langle E \rangle(T) + k_B T, \quad (15)$$

where k_B is Boltzmann's constant; $\langle E' \rangle(T)$ and $\langle E \rangle(T)$ are the average energy of the transition state (TS) and the average energy of all molecules, respectively. We denote $\Delta E_{\text{corr}} = \langle E' \rangle - \langle E \rangle$ as the Tolman's correction factor. We have recently demonstrated that this correction factor, ΔE_{corr} , strongly depends on the value of the pre-exponential factor, A (Laskin et al., 2002b; Laskin & Futrell, 2003c). The correction factor is quite small for unimolecular reactions, for which pre-exponential factors are in the range 10^{10} – 10^{16} sec^{-1} . However, when dissociation is characterized by very low or very high pre-exponential factors Tolman's correction becomes quite significant (e.g., Tolman's correction factor is close to 3 kcal/mol for $\log(A)$ of 16.2 and increases to 36.4 kcal/mol for $\log(A)$ of 39.2) with the result that the Arrhenius activation energy is strongly correlated with the pre-exponential factor.

Correlation between the Arrhenius parameters is a direct consequence of the relative change in the spacing between vibrational levels of the reactant and the TS and is a function of the degree of tightness/looseness of the TS. Large pre-exponential factors are associated with reactions proceeding via very loose TSs. In this case, the spacing between vibrational levels in the TS is decreased relatively to the reactant molecule. This results in a higher average energy of the TS and positive correction factor, meaning that the Arrhenius activation energy is higher than the threshold energy for the reaction. For reactions proceeding via a very tight TS (low pre-exponential factors) ΔE_{corr} is negative and the Arrhenius activation energy is lower than the threshold energy.

The strong correlation between the Arrhenius parameters can reverse the order of Arrhenius activation energies for different systems relative to the order of the corresponding threshold energies. It follows that knowledge of both the Arrhenius activation energy and the pre-exponential factor is required to deduce the actual dissociation energetics based on Tolman's theorem.

IV. SURFACE-INDUCED DISSOCIATION

In contrast with IRMPD and SORI-CID that involve slow step-wise excitation of the ion, ion-surface impact results in almost instantaneous energy deposition. SID is a very powerful tool to probe structures and fragmentation mechanisms of large molecules (Dongre, Somogyi, & Wysocki, 1996). Physical and chemical processes occurring during collisions of low-energy (1–100 eV) polyatomic ions with different surfaces have been recently reviewed (Grill et al., 2001). During ion-surface collision part of ion kinetic energy (typically 5–35%) is converted into the internal energy resulting in efficient activation of the precursor ion on a timescale of a few picoseconds. A detailed discussion of the efficiency of energy transfer in SID has been presented elsewhere (Laskin & Futrell, 2003a) and will not be repeated in this review.

Extremely fast ion activation distinguishes SID from other activation techniques for large molecules. Similarly to IRMPD, SID does not require the introduction of collision gas into the ICR cell for ion activation and removing it prior to mass analysis, dramatically shortening the acquisition time for MS/MS experiments. However, in contrast to IRMPD SID is mass selective, i.e., only one precursor ion is excited by collision. In addition, trapping of scattered ions and their fragments in a strong magnetic field ensures efficient integration over all scattering angles, resulting in high collection efficiency. Finally, because SID does not require any rf excitation it does not produce any “blind” spots. It follows that SID combines all possible advantages of SORI-CID and IRMPD. It is, therefore, interesting to understand why SID has been largely ignored by FT-ICR practitioners.

In the following section, we will discuss instrumental implementation of SID in FT-ICR MS with brief discussion of the in-trap SID and a more detailed consideration of SID of externally produced and mass selected ions. We will show that external mass selection and accumulation of ions is an important prerequisite for SID in FT-ICR. These techniques have been developed in the last 5 years for applications in proteomics and high-throughput FT-ICR MS (Senko et al., 1997; Belov et al., 2001a). Most new commercial FT-ICR instruments are now equipped with these or similar capabilities.

A. Implementation of SID in FT-ICR MS

1. SID With in-Trap Mass Selection of the Precursor Ion

Initial FT-ICR SID experiments involved in-trap mass selection of ions followed by acceleration of mass-selected ions towards the surface. This strategy was utilized in several early studies (James & Wilkins, 1990; Chorush et al., 1995), in which ions were collided with a surface by floating the cell plates and one of the trapping plates or by applying a voltage pulse to either of the trapping plates. Chorush et al. (1995) demonstrated the utility of SID for analyzing large peptides and proteins in FT-ICR MS. However, SID of ions previously stored in the ICR cell resulted in a very poor collection efficiency of fragment ions, low-quality MS/MS spectra, and poorly defined collision energy and incidence angle. Furthermore, pulsed gas introduction was required to confine ions to the center of the cell prior to detection, making

the acquisition time for SID experiments comparable or even longer than for SORI-CID experiments. These findings collectively lead to the conclusion that SID is not suitable for FT-ICR experiments.

2. SID of Externally Produced Mass-Selected Ions

Alternatively, ions produced and mass selected in an external source can be impacted on a surface and their fragments stored in the ICR cell using gated trapping. This approach was previously implemented by our group on two commercial FT-ICR mass spectrometers (Zhong et al., 1997; Rakov et al., 2000; Rakov et al., 2002a,b). In these studies, the SID target was positioned at the rear trapping plate of the ICR cell resulting in normal-incidence collisions of ions with the surface. The collision energy, defined by the potential difference between the ion source offset and the voltage applied to the surface, was varied by changing the bias voltage applied to the ion source. Although both collision energy and impact angle are well defined in this case, some defocusing of ion beam by electrostatic ion transfer optics occurs as a result of biasing the ion source at different voltages. This can result in poor transmission of ion transfer optics at higher collision energies. This deficiency both compromises quantitative studies and makes it difficult to adopt this approach for FT-ICR systems that use different types of superconducting magnets and different types of ion transfer optics. We note that this approach worked rather efficiently on older instruments equipped with unshielded or passively shielded magnets because a more gradual transition of magnetic field strength assists ion transmission, enhances ion focusing, and reduces the dependence of transmission efficiency on the initial focusing of the ion beam.

Another important drawback of these earlier experiments was the lack of mass selection in the external electrospray source of older commercial FT-ICR instruments. This was overcome by using clean samples that exclusively produced ions corresponding to a single peptide. However, it was difficult to separate a single charge state for larger peptides. The charge state distribution could be affected during ion accumulation in an external hexapole and additional mass-selection was achieved by adjusting the time delay between ion extraction from the hexapole and the gated trapping. This accounted for differences in flight times of different charge states of the same peptide through the ion guide. However, the mass resolution that could be achieved using this approach was very poor (Rakov et al., 2000). Our new instrument described in detail elsewhere (Laskin et al., 2002a) utilizes a high-transmission electrospray interface along with a commercial mass-resolving quadrupole and an accumulation quadrupole used for pre-concentration of precursor ions and their thermalization. Ions extracted from the accumulation quadrupole have a fairly narrow distribution of kinetic energies and a nearly thermal distribution of internal energies.

An additional advantage of our new apparatus is that kinetic energy of ions impacting the surface is controlled by a DC offset applied to the ICR cell (Laskin et al., 2002a). This is a significant improvement over our previous work because the final kinetic energy of precursor ions is changed in a strong magnetic field and ion beam trajectories are unperturbed by the deceleration optics.

This is achieved by capacitive coupling of excitation plates to the desired DC bias potential and offsetting the ground of the preamplifier to the same potential. The cell and surface potential can be varied between -150 and $+150$ V. The SID surface is introduced to the rear trapping plate of the ICR cell using a custom probe and vacuum-lock system. Ions are extracted from the electrospray interface into an electrostatic ion guide, transferred through the ICR cell, and collided with a surface at normal incidence. Scattered ions are trapped using gated trapping in a specially fabricated cylindrical ICR cell designed to eliminate the fourth order term in the electrostatic trapping field (Tinkle & Barlow, 2002). It has been demonstrated that such a quadratic trap can be operated with much higher trapping voltages than conventional ICR cells without degrading the cell performance. This setup allows us to obtain high quality single-scan SID spectra in less than 0.2 sec (Laskin et al., 2002a) as compared to a typical acquisition time of approximately 5 sec for SORI-CID experiments. An example of the quality of SID spectra is given in Figure 22.

The system described above has optimal flexibility for SID experiments in FT-ICR. However, it should be noted that the simpler approach adopted in our earlier studies or its straightforward adaptations can be easily utilized to perform SID on commercial instruments.

B. Fundamental Principles of SID

1. Kinetic Energy of Scattered Ions

The success of the experimental approach described above relies on the fact that ions scattered off the surface have very low kinetic energies. Kinetic energy distributions of scattered ions have been measured for benzene and $\text{Cr}(\text{CO})_6^+$ as precursor ions (Rakov et al., 2000; Rakov & Futrell, 2002). For $\text{Cr}(\text{CO})_6^+$ and its fragments the most probable kinetic energy of scattered ions is lower than 1 eV and the distributions are fairly narrow (<2 eV FWHM). Kinetic energy distributions of ions derived from benzene are centered at approximately 4 eV (Rakov et al., 2000). However, it has been demonstrated that these distributions have been biased by the potential difference between the surface and the ICR cell (Rakov & Futrell, 2002). Therefore, the most probable energy for benzene fragments has been significantly overestimated. Clearly the recoil energy of ions from such SAM surfaces is quite low.

The most precise information on recoil kinetic energy of fragment ions from SAM surfaces to date has been obtained from beam measurements analogous to those described earlier for gas phase experiments. In particular, the neutral crossed beam assembly is replaced by a surface mounted at various angles with respect to the ion beam. Results from such an experiment for acetone molecular ions impacted on the same fluorinated SAM surface utilized in our FT-ICR experiments have recently been published (Shukla & Futrell, 2003). Figure 21 shows as a typical example the angular velocities of acetyl ions resulting from the reactive scattering of acetone molecular ions impacted at 45° on the SAM surface at a laboratory collision energy of 25.2 eV. Three dynamically distinct mechanisms are observed, one in which very little ion kinetic energy is lost (3) and two in which

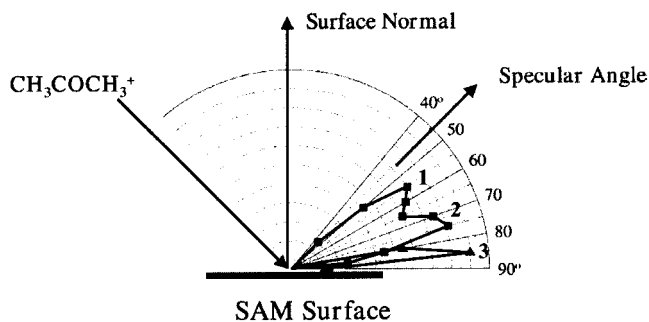


FIGURE 21. Velocity vector distribution of acetyl ions from surface-induced dissociation (SID) of acetone cations on a fluorinated self-assembled monolayer on gold {111} at 25 eV collision energy showing angular distributions and kinetic energies of recoiling ions. Three dynamically distinct mechanisms are observed, one in which very little ion kinetic energy is lost (3) and two in which nearly all of the ion's initial kinetic energy is transferred into the SAM (1 and 2). Kinetic energies of scattered ions for these three processes are as follows: (1) $E_{\perp} = 0.3$ eV, $E_{\parallel} = 0.6$ eV; (2) $E_{\perp} = 0.2$ eV, $E_{\parallel} = 2$ eV; (3) $E_{\perp} = 0.2$ eV, $E_{\parallel} = 24$ eV.

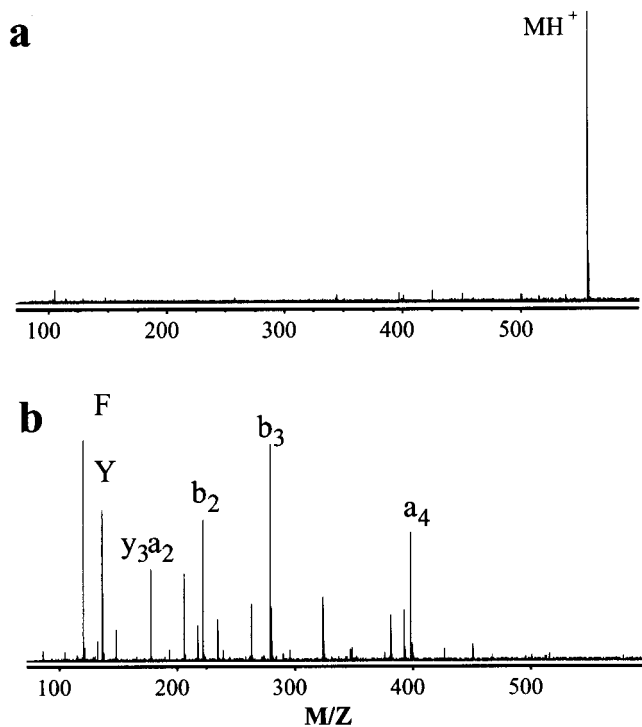


FIGURE 22. SID mass spectra of protonated leucine enkephalin obtained in the pulsed mode with 0.2 sec accumulation in the AQ at 7×10^{-4} Torr. The SID collision energy is (a) 5 eV and (b) 30 eV. Reproduced from Laskin et al. (2002a), with permission from American Chemical Society, copyright 2002.

nearly all of the ion's initial kinetic energy is transferred into the SAM (1 and 2). All three mechanisms result in very low recoil energy normal to the surface—0.3, 0.2, and 0.2 eV, respectively, starting with the peak closest to the specular angle in Figure 21. Interestingly, the kinetic energy component parallel to the surface is very different for the three features—0.6, 2, and 24 eV for mechanisms 1, 2, and 3, respectively. Similar dynamics are observed for other simple molecular ions and for atomic ions scattered from these surfaces. The transfer of large amounts of ion kinetic energy into the surface is not unexpected, since gas phase collisions with molecular targets transfer less energy into the ion and more into the neutral than when atomic targets are used. The SAM surface is an extreme example of a neutral collider with many internal degrees of freedom.

2. Energy Transfer and Shattering of Peptide Ions on Surfaces

This topic has been extensively reviewed (Laskin, Bailey, & Futrell, 2003; Laskin & Futrell, 2003a) and will be only briefly outlined here for clarity. It has been reported that in many cases SID results in very similar fragmentation pattern as SORI-CID (Laskin, Denisov, & Futrell, 2001). Modeling of collision energy-resolved SID data demonstrated that similarly to SORI-CID ion impact on the surface results in deposition of a quasi-thermal distribution of internal energies and peptide decomposition is accurately described using statistical RRKM theory. However, with increasing complexity of the ion the amount of internal energy that can be stored in its internal modes prior to dissociation increases. This is particularly important for species that undergo kinetically unfavored (slow) dissociation. Interestingly, we have discovered that a very fast fragmentation channel opens up at internal energies in excess of 10 eV. The fast fragmentation is adequately described within the so-called "sudden death" approximation, according to which molecule fragments instantaneously after reaching a certain threshold. The transition from slow statistical dissociation to very fast fragmentation at higher collision energies was attributed to shattering of ions on surfaces (Laskin, Bailey, & Futrell, 2003).

The shattering transition has been previously observed and quantified for cluster ions and small molecules (Raz, Even, & Levine, 1995; Hendell, Even, Raz, & Levine, 1995; Raz & Levine, 1996; Beck et al., 1996a,b; Campbell, Raz, & Levine, 1996; Schultz & Hanley, 1998; Kaiser et al., 1999). It has also been predicted in trajectory simulations for collisions of protonated glycine with diamond surface (Meroueh, Wang, & Hase, 2002). Shattering of peptide ions opens up a variety of dissociation pathways that cannot be accessed using slow ion activation and results in formation of mainly backbone fragments including a large number of internal fragments and immonium ions. A potential application of the high-energy SID is identification of singly protonated ions produced by MALDI. It is well known that in many cases singly protonated ions produce poor MS/MS spectra. This is a direct consequence of very slow selective fragmentation at low internal excitations. For example, the only fragments observed for singly protonated des-Arg¹-bradykinin (PPGFSPFR) by slow activation correspond to loss of water and formation of the y₆ ion. These two fragment ions are

also exclusively observed in low-energy (<30 eV) FT-ICR SID. However, at collision energies above 30 eV SID of des-Arg¹-bradykinin produces fragment ions across the entire mass range, resulting in a significant improvement in sequence coverage. We also note that the shattering mechanism is readily accessed by changing the voltage applied to the surface. This enables fast switching between predominantly slow and predominantly fast dissociation.

3. SID Fragmentation Patterns

Most SID spectra of peptides contain b_n and y_n fragment ions, as well as fragment ions resulting from additional losses of H₂O, NH₃, CO and internal fragments. In fact, low-energy SID spectra are very similar to SORI-CID spectra (Laskin, Denisov, & Futrell, 2001; Laskin & Futrell, 2003d). However, shattering opens up numerous dissociation pathways that cannot be accessed using SORI-CID. It should be noted that even at high collision energies (>50 eV) SID mass spectra are dominated by backbone fragmentation. At collision energies in excess of 100 eV mainly immonium ions are observed. For peptide ions of 7–15 residues the most interesting energy regime is from 20 to 60 eV for collisions with fluorinated self-assembled monolayers. The type of fragment ions (b, y, internal) observed in high-energy SID spectra is a strong function of the properties of the peptide ion. For example, whereas high-energy SID spectrum of Fibrinopeptide A is dominated by low-mass ions, high-energy SID spectra of bradykinin, and its analogs contain fragment ions across the entire mass range. Some peptides have a strong propensity to form internal fragments by consecutive dissociation of unstable primary fragment ions, whereas other form internal fragments preferentially by shattering mechanism. We have also found that some fragment ions can be formed both by unimolecular dissociation in the gas phase and shattering. For example, the b₂ ion from des-Arg⁹-bradykinin formed via the lowest-energy pathway at low collision energies contains a substantial contribution from fast decomposition pathway at higher collision energy.

4. Choice of the SID Target

The major drawback of ion activation by collisions with surfaces is the substantial loss of ions on the surface via neutralization or soft landing (Miller et al., 1997). A good SID target should be characterized by a relatively low neutralization efficiency but should be conductive enough to prevent surface charging effects that would perturb potentials close to the surface and alter the kinetic energy of impacting ions. High neutralization efficiencies preclude using clean metal surfaces in SID studies. Organic thin films on metal substrates substantially reduce neutralization of projectile ions. Surfaces commonly used in SID experiments include self-assembled monolayers of *n*-alkanethiols (HSAM) and their fluorinated analogs (FSAM) on gold or silver (Morris et al., 1992; Cooks et al., 1994; Dongre, Somogyi, & Wysocki, 1996), thin films of a liquid perfluoropolyether (Koppers et al., 1997), Langmuir–Blodgett (L–B) films (Gu et al., 1999) or highly oriented pyrolytic graphite (Beck et al., 1996a). Thin films of insulating materials (such as metal halides or diamond) on

metal substrates have a great potential for efficient dissociation of large molecules (Laskin & Futrell, 2003b). It has been estimated that the total yield of ions scattered off fluorocarbon surfaces is approximately 30% (Dongre, Somogyi, & Wysocki, 1996). Our experience with FT-ICR SID using different surfaces suggests that FSAM, HSAM, diamond, and LiF surfaces provide comparable spectral intensities of scattered ions.

Ion loss on surfaces is a strong function of collision energy. The dependence of the total ion current for leucine enkephalin as a projectile ion on the collision energy is shown in Figure 23. The total ion current increases steadily at low collision energies and levels off at energies above 20 eV. The observed dependence of total ion current on collision energy reflects the increased neutralization (or ion capture) probability at low collision energies, most likely resulting from capture of impacting ions by the SAM surface—a dominant process at collision energies below 10 eV (Miller et al., 1997).

Another important consideration for the proper choice of SID target is the efficiency of translational-to-vibrational ($T \rightarrow V$) energy transfer (Laskin & Futrell, 2003a). It is well known that the efficiency of energy transfer is higher for fully or partially fluorinated films than for hydrogen-terminated films. For example, the percent of $T \rightarrow V$ transfer is in the range of 18–28% for FSAM and 12–17% for HSAM surfaces (Cooks et al., 1994; Miller et al., 1994; Dongre, Somogyi, & Wysocki, 1996). Classical trajectory simulations by Hase and co-workers demonstrated that surface stiffness has a major effect of the $T \rightarrow V$ transfer efficiency. According to these simulations collisions of $\text{Cr}(\text{CO})_6^+$ with soft (HSAM) and stiff (diamond) surfaces demonstrated deeper penetration of ion into the HSAM surface resulting in longer times for ion-surface interaction and lower energy transfer (Meroueh & Hase, 2001). Similar trends were predicted for small protonated polyglycines. Namely, diamond is predicted to be two

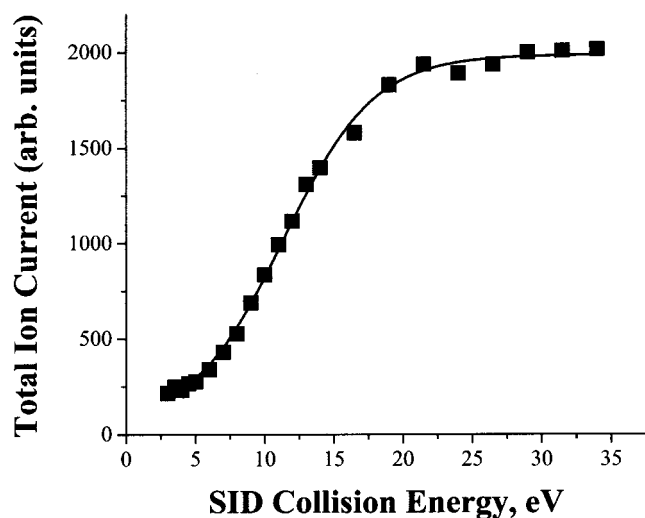


FIGURE 23. Total ion current of ions scattered from the surface as a function of SID collision energy for protonated leucine enkephalin as a precursor ion. Reproduced from Laskin et al. (2002a), with permission from American Chemical Society, copyright 2002.

to three times more efficient than HSAM in collisional excitation of these ions (Meroueh & Hase, 2002).

Our FT-ICR SID studies of collisions of the singly protonated des-Arg¹-bradykinin with different surfaces (Laskin & Futrell, 2003b) demonstrated that the percent of $T \rightarrow V$ transfer increases in the order: HSAM (10.1%), lithium fluoride (12.0%), diamond (19.2%), FSAM (20.5%). In addition, we found that the width of the energy deposition function (EDF) is affected by the properties of the SID target. The shape of EDF for four different surfaces is shown in Figure 24. The EDF for the FSAM surface at 50 eV collision energy is compared to distributions obtained for collisions with the diamond, LiF, and HSAM surfaces at 53, 86, and 102 eV collision energy, respectively. At these collision energies approximately the same most probable internal energy is deposited into the ion. A thermal distribution at 920 K is shown for comparison. The results demonstrate that relatively narrow EDFs are obtained for collisions with the SAM surfaces. Both distributions are well approximated by a thermal distribution of energies, although the FSAM distribution is somewhat closer to thermal. Collisions with stiff crystalline surfaces result in deposition of wider distributions of internal energies. The width of the EDF increases in the order: HSAM < FSAM < LiF < Diamond. We suggested that surface stiffness has a major effect on the width of the EDF, whereas the average energy deposited into the ion is mainly affected by the mass of the chemical moiety constituting the collision partner for the ion impacting the surface.

These findings have several important practical implications. The SID target can be chosen to match a particular application. Specifically, fragmentation of fragile peptides should be

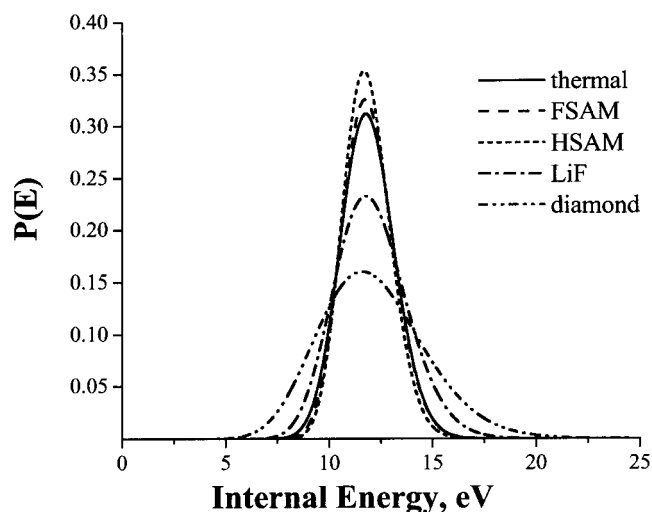


FIGURE 24. Comparison of IEDs resulting in the same most probable internal energy deposition as obtained for 50 eV collisions of singly protonated des-Arg¹-bradykinin with FSAM surface (dashed line). Collision energies are as follows: 53 eV for diamond (dash-dot-dot line), 86 eV for LiF (dash-dot line), and 102 eV for HSAM (dotted line). Thermal distribution (solid line) corresponds to 920 K. Reproduced from Laskin & Futrell (2003b), with permission from American Physical Society, copyright 2003.

better examined using the HSAM or LiF surfaces. For these surfaces the energy transfer efficiency is relatively small and fragmentation occurs at higher collision energies, thereby minimizing ion loss on the surface. For example, leucine enkephalin fragments at less than 10 eV collision energy when the FSAM surface is used as a target. In this energy regime soft landing or neutralization on the surface is the dominant process and the intensity of scattered ions is quite low. However, two times higher collision energy is required to obtain dissociation of leucine enkephalin by collisions with the HSAM surface; this helps to reduce ion loss substantially and improve the signal-to-noise ratio. For most peptides containing more than eight residues fragmentation on FSAM surfaces occurs at collision energies above 20 eV and ion loss on the surface does not present a serious problem.

Different widths of EDF obtained using stiff and soft surfaces can be utilized to vary the sequence coverage obtained in SID spectra. An example of SID spectra obtained on diamond and HSAM surfaces at collision energies resulting in approximately the same average energy deposition is shown in Figure 25. At both collision energies better sequence coverage is obtained for the diamond surface. This is a consequence of the wider EDF, which efficiently averages over the low- and the high-energy dissociation pathways. It follows that while the SAM surfaces

provide a better specificity, which can be advantageous for studying fragmentation mechanisms, stiff crystalline surfaces such as diamond provide a better averaging over different dissociation pathways resulting in a better sequence coverage.

C. Applications

Several studies have demonstrated application of FT-ICR SID for extracting accurate energetics and dynamics of peptide fragmentation (Laskin, Denisov, & Futrell, 2000, 2002; Bailey, Laskin, & Futrell, 2003; Laskin, Bailey, & Futrell, 2003). The advantages provided by SID include very fast ion activation, which eliminates possible discrimination against higher-energy dissociation pathways, and efficient “amplification” of small changes in dissociation parameters (Bailey, Laskin, & Futrell, 2002; Laskin et al., 2002b). For example, the difference between threshold energies for dissociation of des-Arg¹- and des-Arg⁹-bradykinin is only 0.08 eV, while the values of collision energies required for dissociation differ by 4 eV. Two effects contribute to this “amplification” of subtle variations in threshold energies. First, there is a substantial KS for dissociation of ions of this size even on a long time scale of the FT-ICR experiment. The difference in internal energies required for dissociation of des-Arg¹- and des-Arg⁹-bradykinin is 0.8 eV. This corresponds to a

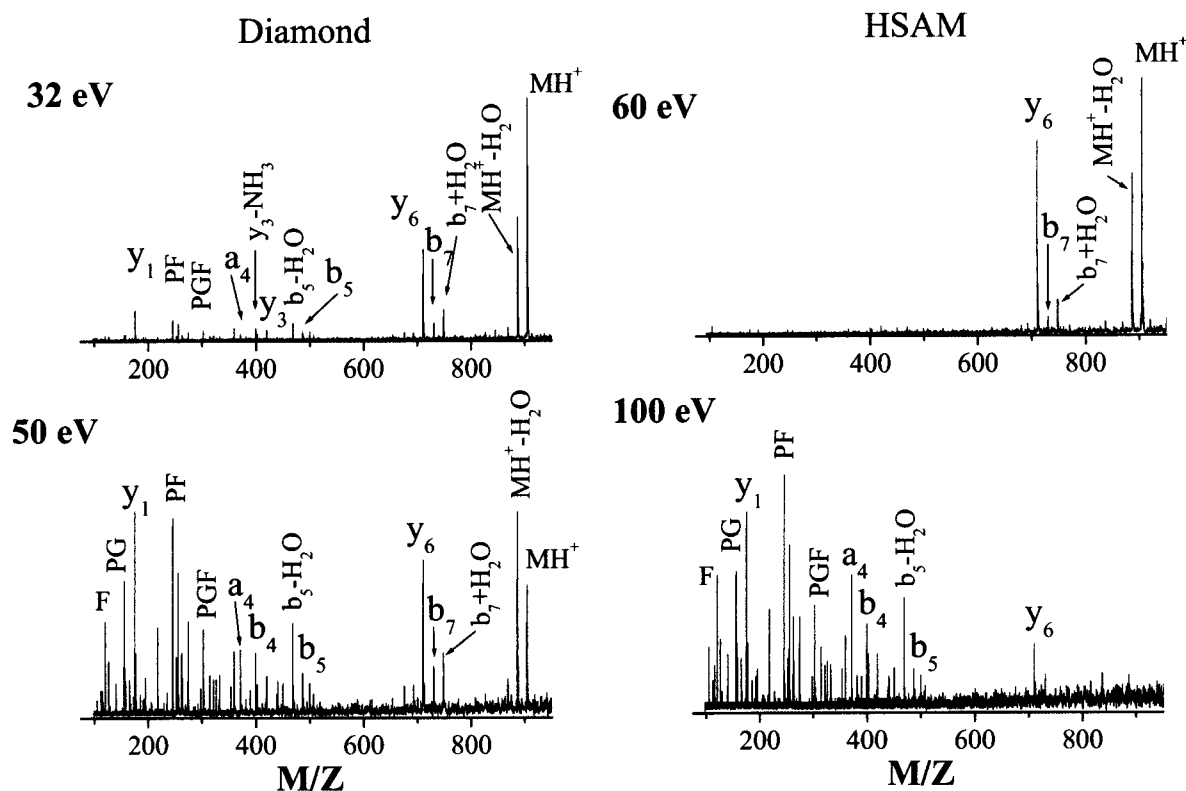


FIGURE 25. SID spectra of des-Arg¹-bradykinin obtained using diamond (left panel) and HSAM (right panel) surfaces. Collision energies were chosen to match the most probable energy deposition for both surfaces. Both at high and low collision energy better sequence coverage is obtained using the diamond surface.

tenfold amplification of differences in threshold energies. Secondly, the $T \rightarrow V$ transfer efficiency is approximately 20%. It follows that the difference in SID collision energies required to observe fragmentation is approximately five times larger than the difference in the corresponding internal energies. Combining these two factors leads to a 50-fold amplification of the energy difference for slowly fragmenting peptides.

Collision energy resolved studies provide important information on the appearance energies of different fragment ions. Another dimension is added to SID experiments by varying the delay between the ion-surface collision and the analysis of resulting fragments to conduct kinetic studies. Although time- and energy-resolved studies have been conducted for only a limited number of peptide ions thus far (Bailey, Laskin, & Futrell, 2002; Laskin, Bailey, & Futrell, 2003), they have demonstrated a great potential for detailed elucidation of fragmentation energetics and mechanisms.

V. SUMMARY

Advancements in ion activation techniques constitute a basis for application of FT-ICR MS for structural characterization of large molecules. In this review, we presented the fundamental aspects of the two established slow activation techniques—SORI-CID and IRMPD. We pointed out on advantages and disadvantages as well as possible combinations of these methods for improving structural information in MS/MS spectra. The third activation method described in this review, SID, has found only a limited application in FT-ICR studies thus far despite clear advantages over both SORI-CID and IRMPD. However, with further development of FT-ICR technology SID may become a method of choice for identification of large molecules.

ACKNOWLEDGMENTS

This work was conducted at the W.R. Wiley Environmental Molecular Sciences Laboratory (EMSL), a national scientific user facility sponsored by the US Department of Energy and located at Pacific Northwest National Laboratory. PNNL is operated by Battelle for the US Department of Energy. Research at EMSL was carried out within the project 40457 supported by the Office of Basic Energy Sciences of the US Department of Energy.

REFERENCES

- Aebersold R, Goodlett DR. 2001. Mass spectrometry in proteomics. *Chem Rev* 101:269–295.
- Amster II. 1996. Fourier transform mass spectrometry. *J Mass Spectrom* 31:1325–1337.
- Bailey TH, Laskin J, Futrell JH. 2003. Energetics of selective cleavage at acidic residues studied by time- and energy-resolved surface-induced dissociation in FT-ICR-MS. *Int J Mass Spectrom* 222:313–327.
- Baykut G, Watson CH, Weller RR, Eyster JR. 1985. Infrared multiphoton dissociation of some oxygen-containing hydrocarbon ions: Differentiation of isomeric ion structures in the gas-phase. *J Am Chem Soc* 107:8036–8042.
- Beck RD, Rockenberger J, Weis P, Kappes MM. 1996a. Fragmentation of C_{60}^+ and higher fullerenes by surface impact. *J Chem Phys* 104:3638–3650.
- Beck RD, Warth C, May K, Kappes MM. 1996b. Surface impact induced shattering of C_{60} . Detection of small Cm fragments by negative surface ionization. *Chem Phys Lett* 257:557–562.
- Belov ME, Nikolaev EN, Anderson GA, Auberry KJ, Harkewicz R, Smith RD. 2001a. Electrospray ionization-Fourier transform ion cyclotron mass spectrometry using ion preselection and external accumulation for ultrahigh sensitivity. *J Am Soc Mass Spectrom* 12:38–48.
- Belov ME, Nikolaev EN, Anderson GA, Udseth HR, Conrads TP, Veenstra TD, Masselon CD, Gorshkov MV, Smith RD. 2001b. Design and performance of an ESI interface for selective external ion accumulation coupled to a Fourier transform ion cyclotron mass spectrometer. *Anal Chem* 73:253–261.
- Berkowitz J. 1979. Photoabsorption, photoionization, and photoelectron spectroscopy. New York: Academic.
- Beu SC, Senko MW, Quinn JP, Wampler FM, McLafferty FW. 1993. Fourier-transform electrospray instrumentation for tandem high-resolution mass-spectrometry of large molecules. *J Am Soc Mass Spectrom* 4:557–565.
- Boering KA, Rolfe J, Brauman JI. 1992. Low-energy collision-induced dissociation: Phase-shifting excitation control of ion kinetic energy in ion-cyclotron resonance spectrometry. *Int J Mass Spectrom Ion Processes* 117:357–386.
- Bomse DS, Berman DW, Beauchamp JL. 1981. Energetics of the rearrangement of neutral and ionized perfluorocyclopropane to perfluoropropylene: Use of infrared multi-photon dissociation spectra to identify structural isomers of molecular-ions. *J Am Chem Soc* 103:3967–3971.
- Bomse DS, Woodin RL, Beauchamp JL. 1979. Molecular activation with low-intensity CW infrared laser radiation. Multiphoton dissociation of ions derived from diethyl ether. *J Am Chem Soc* 101:5503–5512.
- Bomse DS, Beauchamp JL. 1981a. Slow multi-photon excitation as a probe of bimolecular and unimolecular reaction energetics: Multi-photon dissociation of proton bound alcohol dimers. *J Am Chem Soc* 103:3292–3296.
- Bomse DS, Beauchamp JL. 1981b. Infrared photochemistry of $(CH_3)_2Cl^+$, $(CH_3)Cl^+(CD_3)$, and $(CD_3)_2Cl^+$ in the gas-phase using low-intensity cw laser-radiation. *Chem Phys Lett* 77:25–29.
- Bowers WD, Delbert SS, McIver RT. 1986. Consecutive laser-induced photodissociation as a probe of ion structure. *Anal Chem* 58:969–972.
- Bowers WD, Delbert SS, Hunter RL, McIver RT. 1984. Fragmentation of oligopeptide ions using ultraviolet-laser radiation and Fourier-transform mass-spectrometry. *J Am Chem Soc* 106:7288–7289.
- Burlingame AL, Boyd RK, Gaskell SJ. 1998. Mass spectrometry. *Anal Chem* 70:647R–716R.
- Campbell EEB, Raz T, Levine RD. 1996. Internal energy dependence of the fragmentation patterns of C_{60} and C_{60}^+ . *Chem Phys Lett* 253:261–267.
- Cancilla MT, Penn SG, Lebrilla CB. 1998. Alkaline degradation of oligosaccharides coupled with matrix-assisted laser desorption/ionization Fourier transform mass spectrometry: A method for sequencing oligosaccharides. *Anal Chem* 70:663–672.
- Cancilla MT, Wang AW, Voss LR, Lebrilla CB. 1999. Fragmentation reactions in the mass spectrometry analysis of neutral oligosaccharides. *Anal Chem* 71:3206–3218.
- Cheng MH, Chiang MH, Gislason EA, Mahan BH, Tsao CW, Werner AS. 1970. Collisional excitation of small molecular ions. *J Chem Phys* 52:6150–6156.
- Chorush RA, Little DP, Beu SC, Wood TD, McLafferty FW. 1995. Surface-induced dissociation of multiply protonated proteins. *Anal Chem* 67:1042–1046.

- Cooks RG, Ast T, Mabud A. 1990. Collisions of polyatomic ions with surfaces. *Int J Mass Spectrom Ion Processes* 100:209–265.
- Cooks RG, Ast T, Pradeep T, Wysocki V. 1994. Reactions of ions with organic surfaces. *Acc Chem Res* 27:316–323.
- Dienes T, Pastor SJ, Schurch S, Scott JR, Yao J, Cui SL, Wilkins CL. 1996. Fourier transform mass spectrometry: Advancing years (1992–mid1996). *Mass Spectrom Rev* 15:163–211.
- Dongre AR, Somogyi Á, Wysocki VH. 1996. Surface-induced dissociation: An effective tool to probe structure, energetics, and fragmentation mechanisms of protonated peptides. *J Mass Spectrom* 31:339–350.
- Dufresne CP, Wood TD, Hendrickson CL. 1998. High-resolution electrospray ionization Fourier transform mass spectrometry with infrared multiphoton dissociation of glucokinase from *Bacillus stearothermophilus*. *J Am Soc Mass Spectrom* 9:1222–1225.
- Dunbar RC. 1984. Photodissociation in the ICR trap. In: Bowers MT, editor. *Gas phase ion chemistry*. Vol. 3. New York: Academic Press. pp 129–166.
- Dunbar RC. 1991. Kinetics of low-intensity infrared-laser photodissociation: The thermal-model and application of the Tolman theorem. *J Chem Phys* 95:2537–2548.
- Dunbar RC. 2000. Photodissociation of trapped ions. *Int J Mass Spectrom* 200:571–589.
- Dunbar RC, Zaniewski RC. 1992. Infrared multiphoton dissociation of styrene ions by low-power continuous CO₂-laser irradiation. *J Chem Phys* 96:5069–5075.
- Fenn JB, Mann M, Meng CK, Wong SF, Whitehouse CM. 1989. Electrospray ionization for mass-spectrometry of large biomolecules. *Science* 246:64–71.
- Flora JW, Hannis JC, Muddiman DC. 2001. High-mass accuracy of product ions produced by SORI-CID using a dual electrospray ionization source coupled with FTICR mass spectrometry. *Anal Chem* 73:1247–1251.
- Flora JW, Muddiman DC. 2001b. Complete sequencing of mono-deprotonated peptide nucleic acids by sustained off-resonance irradiation collision-induced dissociation. *J Am Soc Mass Spectrom* 12:805–809.
- Flora JW, Muddiman DC. 2001b. Selective, sensitive, and rapid phosphopeptide identification in enzymatic digests using ESI-FTICR-MS with infrared multiphoton dissociation. *Anal Chem* 73:3305–3311.
- Flora JW, Muddiman DC. 2002. Gas-phase ion unimolecular dissociation for rapid phosphopeptide mapping by IRMPD in a penning ion trap: An energetically favored process. *J Am Chem Soc* 124:6546–6547.
- Freitas MA, Hendrickson CL, Marshall AG. 1999. Gas phase activation energy for unimolecular dissociation of biomolecular ions determined by focused radiation for gaseous multiphoton energy transfer (FRAGMENT). *Rapid Commun Mass Spectrom* 13:1639–1642.
- Freitas MA, Hendrickson CL, Marshall AG. 2000. Determination of relative ordering of activation energies for gas-phase ion unimolecular dissociation by infrared radiation for gaseous multiphoton energy transfer. *J Am Chem Soc* 122:7768–7775.
- Futrell JH. 1986. Beam methods. In: Futrell JH, editor. *Gaseous ion chemistry and mass spectrometry*. New York: John Wiley and Sons. pp 155–175.
- Gao JM, Wu QYQ, Carbeck J, Lei QP, Smith RD, Whitesides GM. 1999. Probing the energetics of dissociation of carbonic anhydrase–ligand complexes in the gas phase. *Biophys J* 76:3253–3260.
- Gauthier JW, Trautman TR, Jacobson DB. 1991. Sustained off-resonance irradiation for collision-activated dissociation involving Fourier-transform mass-spectrometry: Collision-activated dissociation technique that emulates infrared multiphoton dissociation. *Anal Chim Acta* 246:211–225.
- Godovac-Zimmermann J, Brown LR. 2001. Perspectives for mass spectrometry and functional proteomics. *Mass Spectrom Rev* 20:1–57.
- Grill V, Shen J, Evans C, Cooks RG. 2001. Collisions of ions with surfaces at chemically relevant energies: Instrumentation and phenomena. *Rev Sci Instrum* 72:3149–3179.
- Grosshans PB, Marshall AG. 1990. Theory of ion-cyclotron resonance mass-spectrometry: Resonant excitation and radial ejection in orthorhombic and cylindrical ion traps. *Int J Mass Spectrom Ion Processes* 100:347–379.
- Gu CG, Wysocki VH, Harada A, Takaya H, Kumadaki I. 1999. Dissociative and reactive hyperthermal ion-surface collisions with Langmuir–Blodgett films terminated by CF₃(CH₂)_n, *n*-perfluoroalkyl, or *n*-alkyl groups. *J Am Chem Soc* 121:10554–10562.
- Guan SH, Marshall AG, Wahl MC. 1994. MS/MS with high detection efficiency and mass resolving power for product ions in Fourier-transform ion-cyclotron resonance mass-spectrometry. *Anal Chem* 66:1363–1367.
- Guan SH, Marshall AG. 1996. Stored waveform inverse Fourier transform (SWIFT) ion excitation in trapped-ion mass spectrometry: Theory and applications. *Int J Mass Spectrom Ion Processes* 158:5–37.
- Guo XH, Grutzmacher HF. 2000. Reactivity and structure of hydrogenated carbon cluster ions C_nH_x⁺ (n = 18, 20, 24; x = 4–12) derived from polycyclic aromatic hydrocarbons by splitting off H center dot atoms: Reactions with dimethyl disulfide. *J Phys Chem A* 104:7811–7820.
- Hakansson K, Cooper HJ, Emmett MR, Costello CE, Marshall AG, Nilsson CL. 2001. Electron capture dissociation and infrared multiphoton dissociation MS/MS of an *N*-glycosylated tryptic peptide to yield complementary sequence information. *Anal Chem* 73 18:4530–4536.
- Hannis JC, Muddiman DC. 2002. Tailoring the gas-phase dissociation and determining the relative energy of activation for dissociation of 7-deaza purine modified oligonucleotides containing a repeating motif. *Int J Mass Spectrom* 219:139–150.
- Heck AJR, Derrick PJ. 1997. Ultrahigh mass accuracy in isotope-selective collision-induced dissociation using correlated sweep excitation and sustained off-resonance irradiation: A Fourier transform ion cyclotron resonance mass spectrometry case study on the [M+2H]²⁺ ion of bradykinin. *Anal Chem* 69:3603–3607.
- Heck AJR, Derrick PJ. 1998. Selective fragmentation of single isotopic ions of proteins up to 17 kDa using 9.4 Tesla Fourier transform ion cyclotron resonance. *Eur Mass Spectrom* 4:181–188.
- Heck AJR, Dekoning LJ, Pinkse FA, Nibbering NMM. 1991. Mass-specific selection of ions in Fourier-transform ion-cyclotron resonance mass-spectrometry: Unintentional off-resonance cyclotron excitation of selected ions. *Rapid Commun Mass Spectrom* 5:406–414.
- Hendell E, Even U, Raz T, Levine RD. 1995. Shattering of clusters upon surface impact: An experimental and theoretical-study. *Phys Rev Lett* 75:2670–2673.
- Herman Z, Futrell JH, Friedrich B. 1984. A beam scattering study of the collision-induced dissociation of polyatomic ions CH₄⁺ and C₃H₈⁺ at eV collision energies. *Int J Mass Spectrom Ion Processes* 58:181–199.
- Hettich RL, Stemmler EA. 1996. Investigation of oligonucleotide fragmentation with matrix-assisted laser desorption ionization Fourier-transform mass spectrometry and sustained off-resonance irradiation. *Rapid Commun Mass Spectrom* 10:321–327.
- Hillenkamp F, Karas M, Beavis RC, Chait BT. 1991. Matrix-assisted laser desorption ionization mass-spectrometry of biopolymers. *Anal Chem* 63:A1193–A1202.
- Hofstadler SA, Sannes-Lowery KA, Griffey RH. 1999. Infrared multiphoton dissociation in an external ion reservoir. *Anal Chem* 71:2067–2070.
- Hofstadler SA, Sannes-Lowery KA, Griffey RH. 2001. *m/z*-selective infrared multiphoton dissociation in a Penning trap using sidekick trapping and an rf-tickle pulse. *Rapid Commun Mass Spectrom* 15:945–951.
- Hofstadler SA, Wahl JH, Bakhtiar R, Anderson GA, Bruce JE, Smith RD. 1994. Capillary electrophoresis Fourier-transform ion-cyclotron resonance mass-spectrometry with sustained off-resonance irradiation for the characterization of protein and peptide mixtures. *J Am Soc Mass Spectrom* 5:894–899.
- Hofstadler SA, Griffey RH, Pasa-Tolic L, Smith RD. 1998. The use of a stable internal mass standard for accurate mass measurements of

- oligonucleotide fragment ions using electrospray ionization Fourier transform ion cyclotron resonance mass spectrometry with infrared multiphoton dissociation. *Rapi Commun Mass Spectrom* 12:1400–1404.
- Huang YQ, Freiser BS. 1993. Multiphoton infrared photoinduced ion molecule reactions in the gas-phase. *J Am Chem* 115:737–742.
- Huang YL, Pasatolic L, Guan SH, Marshall AG. 1994. Collision-induced dissociation for mass-spectrometric analysis of biopolymers: High-resolution Fourier-transform ion-cyclotron resonance MS(4). *Anal Chem* 66:4385–4389.
- Ijames CF, Wilkins CL. 1990. Surface-induced dissociation by Fourier-transform mass-spectrometry. *Anal Chem* 62:1295–1299.
- Jacobs DC. 2002. Reactive collisions of hyperthermal energy molecular ions with solid surfaces. *Annu Rev Phys Chem* 53:379–407.
- Jasinski JM, Rosenfeld RN, Meyer FK, Brauman JI. 1982. Infrared photochemistry of $[(C_2H_5)_2O]_2H^+$ and $C_3F_6^+$: A comparison of pulsed and continuous-wave laser photo-dissociation methods. *J Am Chem Soc* 104:652–658.
- Jockusch RA, Paech K, Williams ER. 2000. Energetics from slow infrared multiphoton dissociation of biomolecules. *J Phys Chem A* 104:3188–3196.
- Kaiser B, Bernhardt TM, Stegemann B, Opitz J, Rademann K. 1999. Bimodal distribution in the fragmentation behavior of small antimony clusters Sb_x^+ ($x = 3–12$) scattered from a highly oriented pyrolytic graphite surface. *Phys Rev Lett* 83:2918–2921.
- Kim MS. 1983. Fragmentation probability in collisional-activation mass-spectrometry (CA MS). 1. Effects of sequential collisional excitation. *Int J Mass Spectrom Ion Processes* 50:189–203.
- Koppers WR, Beijersbergen JHM, Weeding TL, Kistemaker PG, Kleyn AW. 1997. Dissociative scattering of polyatomic ions from a liquid surface: CF_3^+ on a perfluoropolyether film. *J Chem Phys* 107:10736–10750.
- Koster S, Duursma MC, Boon JJ, Nielen MWF, de Koster CG, Heeren RMA. 2000. Structural analysis of synthetic homo- and copolyesters by electrospray ionization on a Fourier transform ion cyclotron resonance mass spectrometer. *J Mass Spectrom* 35:739–748.
- Kruppa G, Schmier PD, Tabei K, Van Orden S, Siegel MM. 2002. Multiple ion isolation applications in FT-ICR MS: Exact-mass MS^n internal calibration and purification/interrogation of protein–drug complexes. *Anal Chem* 74:3877–3886.
- Laskin J, Bailey TH, Futrell JH. 2003. Shattering of peptide ions on self-assembled monolayer surfaces. *J Am Chem Soc* 125:1625–1632.
- Laskin J, Byrd M, Futrell J. 2000. Internal energy distributions resulting from sustained off-resonance excitation in FTMS: I. Fragmentation of the bromobenzene radical cation. *Int J Mass Spectrom* 196:285–302.
- Laskin J, Denisov E, Futrell JH. 2000. A comparative study of collision-induced and surface-induced dissociation. 1. Fragmentation of protonated dialanine. *J Am Chem Soc* 122:9703–9714.
- Laskin J, Denisov E, Futrell JH. 2001. Comparative study of collision-induced and surface-induced dissociation. 2. Fragmentation of small alanine-containing peptides in FT-ICR MS. *J Phys Chem B* 105:1895–1900.
- Laskin J, Denisov E, Futrell JH. 2002. Fragmentation energetics of small peptides from multiple-collision activation and surface-induced dissociation in FT-ICR MS. *Int J Mass Spectrom* 219:189–201.
- Laskin J, Futrell J. 2000. Internal energy distributions resulting from sustained off-resonance excitation in FT-ICR MS: II. Fragmentation of the 1-bromonaphthalene radical cation. *J Phys Chem A* 104:5484–5494.
- Laskin J, Futrell JH. 2002. On the efficiency of energy transfer in collisional activation of small peptides. *J Chem Phys* 116:4302–4310.
- Laskin J, Futrell JH. 2003a. Collisional activation of peptide ions in FT-ICR mass spectrometry. *Mass Spectrom Rev* 22:158–181.
- Laskin J, Futrell JH. 2003b. Energy transfer in collisions of peptide ions with surfaces. *J Chem Phys* 119:3413–3420.
- Laskin J, Futrell JH. 2003c. Entropy is the major driving force for fragmentation of proteins and protein–ligand complexes in the gas-phase. *J Phys Chem A* 107:5836–5839.
- Laskin J, Futrell JH. 2003d. Surface-induced dissociation of peptide ions: Kinetics and dynamics. *J Am Soc Mass Spectrom* 14:1340–1347.
- Laskin J, Denisov EV, Shukla AK, Barlow SE, Futrell JH. 2002a. Surface-induced dissociation in a Fourier transform ion cyclotron resonance mass spectrometer: New instrument design and evaluation. *Anal Chem* 74:3255–3261.
- Laskin J, Bailey TH, Denisov EV, Futrell JH. 2002b. On the relative stability of singly protonated des-Arg1 and des-Arg9 bradykinins. *J Phys Chem A* 106:9832–9836.
- Leavell MD, Kruppa GH, Leary JA. 2002. Analysis of phosphate position in hexose monosaccharides using ion-molecule reactions and SORI-CID on an FT-ICR mass spectrometer. *Anal Chem* 74:2608–2611.
- Lee SH, Kim MS, Beynon JH. 1987. Proposal for an analytical form of the collisional energy deposition probability. *Int J Mass Spectrom Ion Processes* 75:83–89.
- Lee SA, Jiao CQ, Huang YQ, Freiser BS. 1993. Multiple excitation collisional activation in Fourier-transform mass-spectrometry. *Rapid Commun Mass Spectrom* 7:819–821.
- Levine RD, Bernstein RB. 1987. Molecular reaction dynamics and chemical reactivity. Oxford: University Press.
- Li WQ, Hendrickson CL, Emmett MR, Marshall AG. 1999. Identification of intact proteins in mixtures by alternated capillary liquid chromatography electrospray ionization and LC ESI infrared multiphoton dissociation Fourier transform ion cyclotron resonance mass spectrometry. *Anal Chem* 71:4397–4402.
- Li LJ, Masselon CD, Anderson GA, Pasa-Tolic L, Lee SW, Shen YF, Zhao R, Lipton MS, Conrads TP, Tolic N, Smith RD. 2001. High-throughput peptide identification from protein digests using data-dependent multiplexed tandem FTICR mass spectrometry coupled with capillary liquid chromatography. *Anal Chem* 73:3312–3322.
- Lifshitz C. 1992. Recent developments in applications of RRKM-QET. *Int J Mass Spectrom Ion Processes* 118:315–337.
- Lifshitz C. 2002. Kinetic shifts. *Eur J Mass Spectrom* 8:85–92.
- Little DP, McLafferty FW. 1996. Infrared photodissociation of non-covalent adducts of electrosprayed nucleotide ions. *J Am Soc Mass Spectrom* 7:209–210.
- Little DP, Speir JP, Senko MW, O'Connor PB, McLafferty FW. 1994. Infrared multiphoton dissociation of large multiply charged ions for biomolecule sequencing. *Anal Chem* 66:2809–2815.
- Little DP, Aaserud DJ, Valaskovic GA, McLafferty FW. 1996. Sequence information from 42–108-mer DNAs (complete for a 50-mer) by tandem mass spectrometry. *J Am Chem Soc* 118(39):9352–9359.
- Liu CL, Tolic LP, Hofstadler SA, Harms AC, Smith RD, Kang CH, Sinha N. 1996. Probing regA/RNA interactions using electrospray ionization Fourier transform ion cyclotron resonance-mass spectrometry. *Anal Biochem* 262:67–76.
- Lupo DW, Quack M. 1987. IR-laser photochemistry. *Chem Rev* 87:181–216.
- Mabud MDA, Dekrey MJ, Cooks RG. 1985. Surface-induced dissociation of molecular-ions. *Int J Mass Spectrom Ion Processes* 67:285–294.
- Maier CS, Yan XG, Harder ME, Schimerlik MI, Deinzer ML, Pasa-Tolic L, Smith RD. 2000. Electrospray ionization Fourier transform ion cyclotron resonance mass spectrometric analysis of the recombinant human macrophage colony stimulating factor beta and derivatives. *J Am Soc Mass Spectrom* 11:237–243.
- Mann M, Hendrickson RC, Pandey A. 2001. Analysis of proteins and proteomes by mass spectrometry. *Ann Rev Biochem* 70:437–473.
- Marshall AG. 2000. Milestones in Fourier transform ion cyclotron resonance mass spectrometry technique development. *Int J Mass Spectrom* 200:331–356.

- Marshall AG, Hendrickson CL, Jackson GS. 1998. Fourier transform ion cyclotron resonance mass spectrometry: A primer. *Mass Spectrom Rev* 17:1–35.
- Marzluff EM, Beauchamp JL. 1996. Collisional activation studies of large molecules. In: Baer T, editor. *Large ions: Their vaporization, detection, and structural analysis*. New York: John Wiley & Sons. pp 115–143.
- Masselon C, Anderson GA, Harkewicz R, Bruce JE, Pasa-Tolic L, Smith RD. 2000. Accurate mass multiplexed tandem mass spectrometry for high-throughput polypeptide identification from mixtures. *Anal Chem* 72:1918–1924.
- McLafferty FW. 1994. High-resolution tandem FT mass-spectrometry above 10-kDa. *Acc Chem Res* 27:379–386.
- McLafferty FW, Guan ZQ, Haupts U, Wood TD, Kelleher NL. 1998. Gaseous conformational structures of cytochrome c. *J Am Chem Soc* 120:4732–4740.
- McLucky SA. 1992. Principles of collisional activation in analytical mass-spectrometry. *J Am Soc Mass Spectrom* 3:599–614.
- McLucky SA, Goeringer DE. 1997. Slow heating methods in tandem mass spectrometry. *J Mass Spectrom* 32:461–474.
- Meroueh SO, Wang YF, Hase WL. 2002. Direct dynamics simulations of collision- and surface-induced dissociation of *N*-protonated glycine. Shattering fragmentation. *J Phys Chem A* 106:9983–9992.
- Meroueh O, Hase WL. 1999. Collisional activation of small peptides. *J Phys Chem A* 103:3981–3990.
- Meroueh O, Hase WL. 2001. Effect of surface stiffness on the efficiency of surface-induced dissociation. *Phys Chem Chem Phys* 3:2306–2314.
- Meroueh O, Hase WL. 2002. Dynamics of energy transfer in peptide-surface collisions. *J Am Chem Soc* 124:1524–1531.
- Miller SA, Riederer DE, Cooks RG, Cho WR, Lee HW, Kang H. 1994. Energy disposal and target effects in hyperthermal collisions of ferrocene molecular-ions at surfaces. *J Phys Chem* 98:245–251.
- Miller SA, Luo H, Pachuta SJ, Cooks RG. 1997. Soft-landing of polyatomic ions at fluorinated self-assembled monolayer surfaces. *Science* 275:1447–1450.
- Mirgorodskaya E, O'Connor PB, Costello CE. 2002. A general method for precalculation of parameters for sustained off resonance irradiation/collision-induced dissociation. *J Am Soc Mass Spectrom* 13:318–324.
- Morris MR, Riederer DE, Winger BE, Cooks RG, Ast T, Chidsey CED. 1992. Ion surface collisions at functionalized self-assembled monolayer surfaces. *Int J Mass Spectrom Ion Processes* 122:181–217.
- Muntean F, Armentrout PB. 2001. Guided ion beam study of collision-induced dissociation dynamics: Integral and differential cross sections. *J Chem Phys* 115:1213–1228.
- Nelson ED, Kentamaa HI. 2001. A Fourier-transform ion cyclotron resonance study of the 3,5-didehydrophenyl cation. *J Am Soc Mass Spectrom* 12:258–267.
- Null AP, Muddiman DC. 2001. Perspectives on the use of electrospray ionization Fourier transform ion cyclotron resonance mass spectrometry for short tandem repeat genotyping in the post-genome era. *J Mass Spectrom* 36:589–606.
- Paech K, Jockusch RA, Williams ER. 2002. Slow infrared laser dissociation of molecules in the rapid energy exchange limit. *J Phys Chem A* 106:9761–9766.
- Pastor SJ, Wilkins CL. 1998. Sustained off-resonance irradiation and collision-induced dissociation for structural analysis of polymers by MALDI-FTMS. *Int J Mass Spectrom* 175:81–92.
- Rakov VS, Futrell JH. 2002. Unimolecular decomposition in ion cyclotron resonance traps: Kinetic energy release and microsecond-scale kinetics. *Eur J Mass Spectrom* 8:252–262.
- Rakov VS, Futrell JH, Denisov EV, Nikolaev EN. 2000. Instrumentation of kinetic energy-resolved surface-induced dissociation in Fourier-transform mass spectrometry. *Eur J Mass Spectrom* 6:299–317.
- Rakov VS, Denisov EV, Laskin J, Futrell JH. 2002a. Surface-induced dissociation of the benzene molecular cation in Fourier transform ion cyclotron resonance mass spectrometry. *J Phys Chem A* 106:2781–2788.
- Rakov VS, Denisov EV, Futrell JH, Ridge DP. 2002b. Surface induced dissociation of chromium hexacarbonyl ion fluorinated alkanethiolate surface in ion cyclotron resonance mass spectrometer: Studies of energetics of the process using recursive internal energy distribution search method. *Int J Mass Spectrom* 213:25–44.
- Raz T, Even U, Levine RD. 1995. Fragment size distribution in cluster-impact: Shattering versus evaporation by a statistical approach. *J Chem Phys* 103:5394–5409.
- Raz T, Levine RD. 1996. On the shattering of clusters by surface impact heating. *J Chem Phys* 105:8097–8102.
- Rodgers MT, Campbell S, Marzluff EM, Beauchamp JL. 1994. Low-energy collision-induced dissociation of deprotonated dinucleotides: Determination of the energetically favored dissociation pathways and the relative acidities of the nucleic-acid bases. *Int J Mass Spectrom Ion Processes* 137:121–149.
- Sannes-Lowery KA, Hofstadler SA. 2000. Characterization of multipole storage assisted dissociation: Implications for electrospray ionization mass spectrometry characterization of biomolecules. *J Am Soc Mass Spectrom* 11:1–9.
- Sannes-Lowery K, Griffey RH, Kruppa GH, Speir JP, Hofstadler SA. 1998. Multipole storage assisted dissociation, a novel in-source dissociation technique for electrospray ionization generated ions. *Rapid Commun Mass Spectrom* 12:1957–1961.
- Schnier PD, Jurchen JC, Williams ER. 1999. The effective temperature of peptide ions dissociated by sustained off-resonance irradiation collisional activation in Fourier transform mass spectrometry. *J Phys Chem B* 103:737–745.
- Schultz DG, Hanley L. 1998. Shattering of SiMe_3^+ during surface-induced dissociation. *J Chem Phys* 109:10976–10983.
- Senko MW, Speir JP, McLafferty FW. 1994. Collisional activation of large multiply charged ions using Fourier-transform mass-spectrometry. *Anal Chem* 66:2801–2808.
- Senko MW, Hendrickson CL, Emmett MR, Shi SDH, Marshall AG. 1997. External accumulation of ions for enhanced electrospray ionization Fourier transform ion cyclotron resonance mass spectrometry. *J Am Soc Mass Spectrom* 8:970–976.
- Shi SDH, Hendrickson CL, Marshall AG, Siegel MM, Kong FM, Carter GT. 1999. Structural validation of saccharomycins by high resolution and high mass accuracy Fourier transform-ion cyclotron resonance-mass spectrometry and infrared multiphoton dissociation tandem mass spectrometry. *J Am Soc Mass Spectrom* 10:1285–1290.
- Shin SK, Beauchamp JL. 1990. Identification of $\text{Mn}(\text{CO})_4\text{CF}_3^-$, $\text{Mn}(\text{CO})_5\text{CF}_3^-$ structural isomers by IR multiphoton dissociation, collision-induced dissociation, and specific ligand displacement-reactions: Studies of the trifluoromethyl migratory decarbonylation reaction in the gas-phase. *J Am Chem Soc* 112:2057–2066.
- Shin SK, Han SJ. 1997. Application of sustained off-resonance irradiation: The beat frequency measurement and radial separation of mass-selected ions. *J Am Soc Mass Spectrom* 8:86–89.
- Shirts RB. 1986. Collision theory and reaction dynamics. In: Futrell JH, editor. *Gaseous ion chemistry and mass spectrometry*. New York: John Wiley & Sons. pp 25–57.
- Shukla AK, Futrell JH. 1993. Collisional activation and dissociation of polyatomic ions. *Mass Spectrom Rev* 12:211–255.
- Shukla AK, Futrell JH. 2000. Tandem mass spectrometry: Dissociation of ions by collisional activation. *J Mass Spectrom* 35:1069–1090.
- Shukla AK, Futrell JH. 2003. Surface-induced dissociation of acetone cations from a self-assembled monolayer surface of fluorinated alkyl thiol on Au (1 1 1) substrate at low collision energies. *Int J Mass Spectrom* 228:563–576.

- Sievers HL, Grutzmacher HF, Caravatti P. 1996. The geometrical factor of infinitely long cylindrical ICR cells for collision energy-resolved mass spectrometry: Appearance energies of EI_2^+ ($E = P, As, Sb, \text{ and } Bi$) from collision-induced dissociation of EI_3^+ and $[EI_2 \cdot \text{ligand}]^+$ complexes. *Int J Mass Spectrom Ion Processes* 158:233–247.
- Solouki T, PasaTolic L, Jackson GS, Guan SG, Marshall AG. 1996. High-resolution multistage MS^2 , and MS^3 matrix-assisted laser desorption/ionization FT-ICR mass spectra of peptides from a single laser shot. *Anal Chem* 68:3718–3725.
- Solouki T, Reinhold BB, Costello CE, O'Malley M, Guan SH, Marshall AG. 1998. Electrospray ionization and matrix-assisted laser desorption/ionization Fourier transform ion cyclotron resonance mass spectrometry of permethylated oligosaccharides. *Anal Chem* 70:857–864.
- Surya PI, Roth LM, Ranatunga DRA, Freiser BS. 1996. Infrared multiphoton dissociation of transition metal containing ions: $MC_nH_{2n}^+$ ($M = Fe, Co, Ni; n = 2-5$). *J Am Chem Soc* 118:1118–1125.
- Thorne LR, Beauchamp JL. 1984. Infrared photochemistry of gas phase ions. In: Bowers MT, editor. *Gas phase ion chemistry*. Vol. 3. New York: Academic Press. pp 41–97.
- Tinkler M, Barlow SE. 2002. "Linearizing" an ion cyclotron resonance cell. *Rev Sci Instr* 73:4185–4200.
- Tolic LP, Bruce JE, Lei QP, Anderson GA, Smith RD. 1998. In-trap cleanup of proteins from electrospray ionization using soft sustained off-resonance irradiation with Fourier transform ion cyclotron resonance mass spectrometry. *Anal Chem* 70:405–408.
- Tonner DS, McMahon TB. 1997. Consecutive infrared multiphoton dissociations in a Fourier transform ion cyclotron resonance mass spectrometer. *Anal Chem* 69:4735–4740.
- Tosh RE, Shukla AK, Futrell JH. 1995. Elaboration of an impulsive model for collision-induced dissociation: Application to $CS_2^+ + Ar \rightarrow S^+ + CS + Ar$. *J Phys Chem* 99:15488–15496.
- Tumas W, Foster RF, Pellerite MJ, Brauman JI. 1983. Isotope effects as a mechanistic probe of unimolecular ion decompositions: Tert-butoxide anion. *J Am Chem Soc* 105:7464–7465.
- Uechi GT, Dunbar RC. 1992. The kinetics of infrared-laser photodissociation of normal-butylbenzene ions at low-pressure. *J Chem Phys* 96:8897–8905.
- Uggerud E, Derrick PJ. 1991. Theory of collisional activation of macromolecules: Impulsive collisions of organic ions. *J Phys Chem* 95:1430–1436.
- Valentine SJ, Counterman AE, Hoaglund-Hyzer CS, Clemmer DE. 1999. Intrinsic amino acid size parameters from a series of 113 lysine-terminated tryptic digest peptide ions. *J Phys Chem B* 103:1203–1207.
- van der Rest G, He F, Emmett MR, Marshall AG, Gaskell SJ. 2001. Gas-phase cleavage of PTC-derivatized electrosprayed tryptic peptides in an FT-ICR trapped-ion cell: Mass-based protein identification without liquid chromatographic separation. *J Am Soc Mass Spectrom* 12:288–295.
- Vanderhart WJ. 1989. Photodissociation of trapped ions. *Mass Spectrom Rev* 8:237–268.
- Vanderhart WJ. 1992. Studies of ion structures by photodissociation. *Int J Mass Spectrom Ion Processes* 118:617–633.
- Wang Y, Shi SDH, Hendrickson CL, Marshall AG. 2000. Mass-selective ion accumulation and fragmentation in a linear octopole ion trap external to a Fourier transform ion cyclotron resonance mass spectrometer. *Int J Mass Spectrom* 198:113–120.
- Watson CH, Baykut G, Eyley JR. 1987. Laser photodissociation of gaseous ions formed by laser desorption. *Anal Chem* 59:1133–1138.
- Williams ER, Furlong JJP, McLafferty FW. 1990. Efficiency of collisionally activated dissociation and 193-nm photodissociation of peptide ions in Fourier-transform mass-spectrometry. *J Am Soc Mass Spectrom* 1:288–294.
- Woodin RL, Bomse DS, Beauchamp JL. 1978. Multiphoton dissociation of molecules with low power continuous wave infrared laser radiation. *J Am Chem Soc* 100:3248–3250.
- Woodward CA, Stace AJ. 1991. Measurements of kinetic-energy release following the unimolecular and collision-induced dissociation of argon cluster ions, Ar_n^+ , for N in the range 2–60. *J Chem Phys* 94:4234–4242.
- Wu QY, Vanorden S, Cheng XH, Bakhtiar R, Smith RD. 1995. Characterization of cytochrome-c variants with high-resolution FT-ICR mass-spectrometry: Correlation of fragmentation and structure. *Anal Chem* 67:2498–2509.
- Wu QY, Cheng XH, Hofstadler SA, Smith RD. 1996. Specific metal-oligonucleotide binding studied by high resolution tandem mass spectrometry. *J Mass Spectrom* 31:669–675.
- Wu QY, Gao JM, JosephMcCarthy D, Sigal GB, Bruce JE, Whitesides GM, Smith RD. 1997. Carbonic anhydrase-inhibitor binding: From solution to the gas phase. *J Am Chem Soc* 119:1157–1158.
- Xie YM, Schubothe KM, Lebrilla CB. 2003. Infrared laser isolation of ions in Fourier transform mass spectrometry. *Anal Chem* 75:160–164.
- Yamada N, Suzuki E, Hirayama K. 2002. Identification of the interface of a large protein-protein complex using H/D exchange and Fourier transform ion cyclotron resonance mass spectrometry. *Rapid Commun Mass Spectrom* 16:293–299.
- Zhong WQ, Nikolaev EN, Futrell JH, Wysocki VH. 1997. Tandem Fourier transform mass spectrometry studies of surface-induced dissociation of benzene monomer and dimer ions on a self-assembled fluorinated alkanethiolate monolayer surface. *Anal Chem* 69:2496–2503.

Julia Laskin is currently a research scientist at the Pacific Northwest National Laboratory (PNNL) in Richland, Washington. She received her M.Sc. degree in Physics from the St. Petersburg (former Leningrad) Polytechnic University in 1990. After immigrating to Israel, she joined the group of Chava Lifshitz for Ph.D. studies focused on unimolecular dissociation of fullerenes and endohedral fullerenes. She completed her Ph.D. degree in 1998 at the Hebrew University of Jerusalem and started her postdoctoral work with Jean Futrell at the University of Delaware. In 1999 she moved to PNNL, where she continued her postdoctoral research with Jean Futrell working on collisional activation and dissociation of large molecules, which remains the major focus of her current research. In addition, she is interested in determination of dissociation energies, reaction entropies, and thermochemical properties for large molecules.

Jean Futrell is Battelle Fellow at the Pacific Northwest National Laboratory (PNNL) in Richland, Washington, the highest scientific rank at the Laboratory. He received his B.S. degree in Chemical Engineering at Louisiana Tech University in 1955 and his Ph.D. at the

University of California at Berkeley in 1958. After serving with the United States Air Force at Wright-Patterson Air Force Base, he began his academic career at the University of Utah in 1966. In 1986 he moved to the University of Delaware as the Willis F. Harrington Professor of Chemistry and Biochemistry and Chair of the Department. He moved to PNNL in 1998 as Director of the W. R. Wiley Environmental Molecular Sciences Laboratory and was appointed Battelle Fellow in 2002. His research interests include development of specialized mass spectrometers, ion–molecule chemistry, and reaction dynamics.